

## The Development of a Novel Nanobody Therapeutic for SARS-CoV-2

Gang Ye <sup>1,\*</sup>, Joseph P. Gallant <sup>2,\*</sup>, Christopher Massey <sup>3</sup>, Ke Shi <sup>4</sup>, Wanbo Tai <sup>5</sup>, Jian Zheng <sup>6</sup>, Abby E. Odle <sup>6</sup>, Molly A. Vickers <sup>6</sup>, Jian Shang <sup>1</sup>, Yushun Wan <sup>1</sup>, Aleksandra Drelich <sup>7</sup>, Kempaiah R. Kempaiah <sup>7</sup>, Vivian Tat <sup>8</sup>, Stanley Perlman <sup>6</sup>, Lanying Du <sup>5</sup>, Chien-Te Tseng <sup>7,9</sup>, Hideki Aihara <sup>4</sup>, Aaron M. LeBeau <sup>2,#</sup>, Fang Li <sup>1,#</sup>

<sup>1</sup>Department of Veterinary and Biomedical Sciences, University of Minnesota, Saint Paul, MN, USA

<sup>2</sup>Department of Pharmacology, University of Minnesota, Minneapolis, MN, USA

<sup>3</sup> Institutional Office of Regulated Nonclinical Studies, University of Texas Medical Branch, Galveston, TX, USA

<sup>4</sup>Department of Biochemistry, Molecular Biology and Biophysics, University of Minnesota, Minneapolis, MN, USA

<sup>5</sup> Laboratory of Viral Immunology, Lindsley F. Kimball Research Institute, New York Blood Center, New York, NY, USA.

<sup>6</sup>Department of Microbiology and Immunology, University of Iowa, Iowa City, IA, USA

<sup>7</sup>Department of Microbiology and Immunology, University of Texas Medical Branch, Galveston, TX, USA

<sup>8</sup> Department of Pathology, University of Texas Medical Branch, Galveston, TX, USA

<sup>9</sup> Center of Biodefense and Emerging Disease, University of Texas Medical Branch, Galveston, TX, USA

\*These authors contributed equally

## # Correspondence:

Fang Li ([lifang@umn.edu](mailto:lifang@umn.edu))

Keywords: COVID-19, single-chain antibody from camelids, spike protein, receptor-binding domain, ACE2, crystal structures, virus neutralization, animal model, drug pharmacokinetics

## Running title: Nanobody therapeutics targeting COVID-19

Impact statement: Potent and low-cost *Nanosota-1* drugs block SARS-CoV-2 infections both *in vitro* and *in vivo* and act both preventively and therapeutically.

42      **Abstract**

43              Combating the COVID-19 pandemic requires potent and low-cost therapeutics.  
44      We identified a novel series of single-domain antibodies (i.e., nanobody), *Nanosota-1*,  
45      from a camelid nanobody phage display library. Structural data showed that *Nanosota-1*  
46      bound to the oft-hidden receptor-binding domain (RBD) of SARS-CoV-2 spike protein,  
47      blocking out viral receptor ACE2. The lead drug possessing an Fc tag (*Nanosota-1C-Fc*)  
48      bound to SARS-CoV-2 RBD with a  $K_d$  of 15.7 picomolar (~3000 times more tightly than  
49      ACE2 did) and inhibited SARS-CoV-2 infection with an  $ND_{50}$  of  
50      0.16 microgram/milliliter (~6000 times more potently than ACE2 did). Administered at a  
51      single dose, *Nanosota-1C-Fc* demonstrated preventive and therapeutic efficacy in  
52      hamsters subjected to SARS-CoV-2 infection. Unlike conventional antibody drugs,  
53      *Nanosota-1C-Fc* was produced at high yields in bacteria and had exceptional  
54      thermostability. Pharmacokinetic analysis of *Nanosota-1C-Fc* documented a greater than  
55      10-day *in vivo* half-life efficacy and high tissue bioavailability. *Nanosota-1C-Fc* is a  
56      potentially effective and realistic solution to the COVID-19 pandemic.

57

58 **Introduction**

59 The novel coronavirus SARS-CoV-2 has led to the COVID-19 pandemic,  
60 devastating human health and the global economy (1, 2). Anti-SARS-CoV-2 drugs are  
61 urgently needed to treat patients, save lives, and revive economies. Yet daunting  
62 challenges confront the development of such drugs. Though small molecule drugs could  
63 theoretically target SARS-CoV-2, they can take years to develop and their use is often  
64 limited by poor specificity and off-target effects. Repurposed drugs, developed against  
65 other viruses, also have low specificity against SARS-CoV-2. Therapeutic antibodies can  
66 be identified and generally have high specificity; however, their expression in  
67 mammalian cells often leads to low yields and high production costs (3, 4). A realistic  
68 therapeutic solution to COVID-19 must be potent and specific, yet easy to produce.

69 Nanobodies are unique antibodies derived from heavy chain-only antibodies  
70 found in members of the camelidae family (llamas, alpacas, camels, etc.) (Fig. S1) (5, 6).  
71 Because of their small size (2.5 nm by 4 nm; 12-15 kDa) and unique binding domains,  
72 nanobodies offer many advantages over conventional antibodies including the ability to  
73 bind cryptic epitopes on their antigen, high tissue permeability, ease of production and  
74 thermostability (7, 8). Although small, nanobodies bind their targets with high affinity  
75 and specificity due to an extended antigen-binding region (7, 8). Furthermore, it has been  
76 documented that they have low toxicity and immunogenicity in humans, if any (7, 8).  
77 One drawback of nanobodies is their quick clearance by kidneys due to their small size;  
78 this can be overcome by adding tags to increase the molecular weight to a desired level.  
79 Underscoring the potency and safety of nanobodies as human therapeutics, a nanobody  
80 drug was recently approved for clinical use in treating a blood clotting disorder (9).

81 Additionally, due to their superior stability, nanobodies can be inhaled to treat lung  
82 diseases (10) or ingested to treat intestine diseases (11). Nanobodies are currently being  
83 developed against SARS-CoV-2 to combat COVID-19 (12, 13). However, to date, none  
84 of the reported nanobodies have been evaluated for therapeutic efficacy *in vivo*.

85 The receptor-binding domain (RBD) of the SARS-CoV-2 spike protein is a prime  
86 target for therapeutic development (14). The spike protein guides coronavirus entry into  
87 host cells by first binding to a receptor on the host cell surface and then fusing the viral  
88 and host membranes (15, 16). The RBDs of SARS-CoV-2 and a closely related SARS-  
89 CoV-1 both recognize human angiotensin-converting enzyme 2 (ACE2) as their receptor  
90 (14, 17-19). Previously, we showed that SARS-CoV-1 and SARS-CoV-2 RBDs both  
91 contain a core structure and a receptor-binding motif (RBM), and that SARS-CoV-2  
92 RBD has significantly higher ACE2-binding affinity than SARS-CoV-1 RBD due to  
93 several structural changes in the RBM (20, 21). We further showed that SARS-CoV-2  
94 RBD is more hidden than SARS-CoV-1 RBD in the entire spike protein as a possible  
95 viral strategy for immune evasion (22). Hence, to block SARS-CoV-2 binding to ACE2,  
96 a nanobody drug would need to bind to SARS-CoV-2 RBD more tightly than ACE2.

97 Here, we report the development of a novel series of anti-SARS-CoV-2 nanobody  
98 therapeutics, *Nanosota-1*. Identified by screening a camelid nanobody phage display  
99 library against the SARS-CoV-2 RBD, the *Nanosota-1* series bound potently to the  
100 SARS-CoV-2 RBD and were effective at inhibiting SARS-CoV-2 infection *in vitro*. The  
101 best performing drug, *Nanosota-1C-Fc*, demonstrated preventative and therapeutic  
102 efficacy in a hamster model of SARS-CoV-2 infection. *Nanosota-1C-Fc* was produced at  
103 high yields easily scalable for mass production and was also found to have a

104 pharmacologically relevant *in vivo* half-life and excellent bioavailability. Our data  
105 suggest that *Nanosota-1c-Fc* may provide an effective solution to the COVID-19  
106 pandemic.

107

108 **Results**

109 ***Nanosota-1* was identified by phage display**

110 For the rapid identification of virus-targeting nanobodies, we constructed a naïve  
111 nanobody phage display library using B cells isolated from the spleen, bone marrow, and  
112 blood of nearly a dozen non-immunized llamas and alpacas (Fig. 1). Recombinant SARS-  
113 CoV-2 RBD, expressed and purified from mammalian cells, was screened against the  
114 library to identify RBD-targeting nanobodies. Select nanobody clones were tested in a  
115 preliminary screen for their ability to neutralize SARS-CoV-2 pseudovirus entry into  
116 target cells (see below for more details about the assay). The nanobody that demonstrated  
117 the highest preliminary neutralization potency was named *Nanosota-1A* and then  
118 subjected to two rounds of affinity maturation. For each round of affinity maturation,  
119 random mutations were introduced to the whole gene of *Nanosota-1A* through error-  
120 prone PCR, and mutant phages were selected for enhanced binding to SARS-CoV-2  
121 RBD. Nanobodies contain four framework regions (FRs) as structural scaffolds and three  
122 complementarity-determining regions (CDRs) for antigen binding. The nanobody after  
123 the first round of affinity maturation, named *Nanosota-1B*, possessed one mutation in  
124 CDR3 and two other mutations in FR3 (near CDR3). Affinity maturation of *Nanosota-1B*  
125 resulted in *Nanosota-1C*, which possessed one mutation in CDR2 and another mutation

126 in FR2. We next made an Fc-tagged version of *Nanosota-1C*, termed *Nanosota-1C-Fc*, to  
127 create a bivalent construct with increased molecular weight.

128 ***Nanosota-1* tightly bound to the SARS-CoV-2 RBD and completely blocked out**  
129 **ACE2**

130 To understand the structural basis for the binding of *Nanosota-1* drugs to SARS-  
131 CoV-2 RBD, we determined the crystal structure of SARS-CoV-2 RBD complexed with  
132 *Nanosota-1C*. The structure showed that *Nanosota-1C* binds close to the center of the  
133 SARS-CoV-2 RBM (Fig. 2A). When the structures of the RBD/*Nanosota-1C* complex  
134 and the RBD/ACE2 complex were superimposed together, significant clashes occurred  
135 between ACE2 and *Nanosota-1C* (Fig. 2B), suggesting that *Nanosota-1C* binding to the  
136 RBD blocks ACE2 binding to the RBD. Moreover, trimeric SARS-CoV-2 spike protein  
137 is present in two different conformations: the RBD stands up in the open conformation  
138 but lies down in the closed conformation (22-24). When the structures of the  
139 RBD/*Nanosota-1C* complex and the closed spike were superimposed together, no clash  
140 was found between RBD-bound *Nanosota-1C* and the rest of the spike protein (Fig.  
141 S2A). In contrast, severe clashes were identified between RBD-bound ACE2 and the rest  
142 of the spike protein in the closed conformation (Fig. S2B). Additionally, neither RBD-  
143 bound *Nanosota-1C* nor RBD-bound ACE2 had clashes with the rest of the spike protein  
144 in the open conformation (Fig. S2C, S2D). Thus, *Nanosota-1C* can access the spike  
145 protein in both its open and closed conformations, whereas ACE2 can only access the  
146 spike protein in its closed conformation. Overall, our structural data reveal that *Nanosota-1C*  
147 is an ideal RBD-targeting drug that not only blocks virus binding to its receptor, but  
148 also accesses its target in the spike protein in different conformations.

149 To corroborate our structural data on the *Nanosota-1*/ACE2 interactions, we  
150 performed binding experiments between *Nanosota-1* drugs and SARS-CoV-2 RBD using  
151 recombinant ACE2 for comparison. The binding affinity between the nanobodies and the  
152 RBD were measured by surface plasmon resonance (Table 1; Fig. S3). *Nanosota-1A*, *-1B*,  
153 *and -1C* bound to the RBD with increasing affinity ( $K_d$  - from 228 nM to 14 nM),  
154 confirming success of the stepwise affinity maturation. *Nanosota-1C-Fc* had the highest  
155 RBD-binding affinity ( $K_d$  - 15.7 pM), which was ~3,000 times tighter than the RBD-  
156 binding affinity of ACE2. Moreover, compared with ACE2, *Nanosota-1C-Fc* bound to  
157 the RBD with a higher  $k_{on}$  and a lower  $k_{off}$ , demonstrating significantly faster binding and  
158 slower dissociation. Next, we investigated the competitive binding among *Nanosota-1C*,  
159 ACE2, and RBD using protein pull-down assay (Fig. S4A). ACE2 and *Nanosota-1C*  
160 were mixed together in different ratios in solution, with the concentration of ACE2 kept  
161 constant; RBD-Fc was added to pull down ACE2 and *Nanosota-1C* from solution. The  
162 result showed that as the concentration of *Nanosota-1C* increased, less ACE2 was pulled  
163 down by the RBD. Thus, ACE2 and *Nanosota-1C* bound competitively to the RBD. We  
164 then analyzed the competitive binding using gel filtration chromatography (Fig. S4B).  
165 ACE2, *Nanosota-1C*, and RBD were mixed, with both ACE2 and *Nanosota-1C* in molar  
166 excess over the RBD. Analysis by gel filtration chromatography documented that no  
167 ternary complex of ACE2, *Nanosota-1C*, and RBD formed; instead, only binary  
168 complexes of RBD/ACE2 and RBD/*Nanosota-1C* were detected. Hence, the bindings of  
169 ACE2 and *Nanosota-1C* to the RBD are mutually exclusive.  
170 ***Nanosota-1C-Fc* potently neutralized SARS-CoV-2 infection *in vitro* and *in vivo***

171 The ability of the *Nanosota-1* drugs to neutralize SARS-CoV-2 infection *in vitro*  
172 was investigated next. Both a SARS-CoV-2 pseudovirus entry assay and authentic SARS-  
173 CoV-2 infection assay were performed (Fig. 3). For the pseudovirus entry assay,  
174 retroviruses pseudotyped with SARS-CoV-2 spike protein (i.e., SARS-CoV-2  
175 pseudoviruses) were used to enter human ACE2-expressing HEK293T cells in the  
176 presence of an inhibitor. The efficacy of the inhibitor was expressed as the concentration  
177 capable of neutralizing 50% of the entry efficiency (i.e., 50% Neutralizing Dose or  
178 ND<sub>50</sub>). *Nanosota-1C-Fc* had an ND<sub>50</sub> for the SARS-CoV-2 pseudovirus of 0.27 µg/ml,  
179 which was ~10 times more potent than monovalent *Nanosota-1C* (2.52 µg/ml) and over  
180 100 times more potent than ACE2 (44.8 µg/ml) (Fig. 3A). Additionally, *Nanosota-1*  
181 drugs potently neutralized SARS-CoV-2 pseudovirus bearing the D614G mutation in the  
182 SARS-CoV-2 spike protein (Fig. S5), which has become prevalent in many strains (25).  
183 For the authentic virus infection assay, live SARS-CoV-2 was used to infect Vero cells in  
184 the presence of an inhibitor. Efficacy of the inhibitor was described as the concentration  
185 capable of reducing the number of virus plaques by 50% (i.e., ND<sub>50</sub>). *Nanosota-1C-Fc*  
186 had an ND<sub>50</sub> of 0.16 µg/ml, which was ~20 times more potent than monovalent  
187 *Nanosota-1C* (3.23 µg/ml) and ~6000 times more potent than ACE2 (980 µg/ml) (Fig.  
188 3B; Fig. S6). Overall, both *Nanosota-1C-Fc* and *Nanosota-1C* are potent inhibitors of  
189 SARS-CoV-2 pseudovirus entry and authentic SARS-CoV-2 infection.

190 After the *in vitro* studies, we next evaluated the therapeutic efficacy of the lead drug  
191 *Nanosota-1C-Fc* in a hamster model challenged with SARS-CoV-2 via intranasal  
192 inoculation. In addition to an untreated control group, three groups of animals were  
193 injected with a single dose of *Nanosota-1C-Fc*: (i) 24 hours pre-challenge at 20 mg/kg

194 body weight, (ii) 4 hours post-challenge at 20 mg/kg, and (iii) 4 hours post-challenge at  
195 10 mg/kg. As previously validated in this model (26), body weight, tissue pathology and  
196 virus titers in nasal swabs were used as metrics of therapeutic efficacy. In the untreated  
197 control group, weight loss was precipitously starting on day 1 post-challenge with the  
198 lowest weight recorded on day 6 (Fig. 4A). Nasal virus titers were high on day 1 and  
199 remained high on day 5 before a decline (Fig. S7). Pathology analysis on tissues collected  
200 on day 10 revealed moderate hyperplasia in the bronchial tubes (i.e., bronchioloalveolar  
201 hyperplasia) (Fig. 4B), with little hyperplasia in the lungs. These data are consistent with  
202 previous reports showing that SARS-CoV-2 mainly infects the nasal mucosa and  
203 bronchial epithelial cells of this hamster model (26). In contrast, hamsters that received  
204 *Nanosota-1C-Fc* 24-hours pre-challenge were protected from SARS-CoV-2, as  
205 evidenced by the metrics of no weight loss, no bronchioloalveolar hyperplasia, and  
206 significantly reduced nasal virus titers (Fig. 4, Fig. S7). When administered 4 hours post-  
207 challenge, *Nanosota-1C-Fc* also effectively protected hamsters from SARS-CoV-2  
208 infections at either dosage (20 or 10 mg/kg), as evidenced by the favorable therapeutic  
209 metrics (Fig. 4, Fig. S7). Overall, *Nanosota-1C-Fc* was effective at combating SARS-  
210 CoV-2 infections both preventively and therapeutically.

211 ***Nanosota-1C-Fc is stable *in vitro* and *in vivo* with excellent bioavailability***

212 With the lead drug *Nanosota-1C-Fc* demonstrating therapeutic efficacy *in vivo*,  
213 we characterized other parameters important to its clinical translation. First, we expressed  
214 *Nanosota-1C-Fc* in bacteria for all the experiments carried out in the current study (Fig.  
215 5A). After purification on protein A column and gel filtration, the purity of *Nanosota-1C-*  
216 *Fc* was nearly 100%. With no optimization, the expression yield reached 40 mg/L of

217 bacterial culture. Second, we investigated the *in vitro* stability of *Nanosota-1C-Fc*  
218 incubated at four temperatures (-80°C, 4°C, 25°C or 37°C) for one week and then  
219 measured the remaining SARS-CoV-2 RBD-binding capacity by ELISA (Fig. 5B). With  
220 -80°C as a baseline, *Nanosota-1C-Fc* retained nearly all of its RBD-binding capacity at  
221 the temperatures surveyed. Third, we measured the *in vivo* stability of *Nanosota-1C-Fc*  
222 (Fig. 5C). *Nanosota-1C-Fc* was injected into mice via tail vein. Sera were obtained at  
223 different time points and measured for their SARS-CoV-2 RBD-binding capacity by  
224 ELISA. *Nanosota-1C-Fc* retained most of its RBD-binding capability after 10 days *in*  
225 *vivo*. Antithetically, *Nanosota-1C* was stable for only several hours *in vivo*. (Fig. S8A).  
226 Last, we examined the biodistribution of *Nanosota-1C-Fc* in mice (Fig. 5D). *Nanosota-*  
227 *1C-Fc* was radiolabeled with zirocinium-89 and injected systemically into mice. Tissues  
228 were collected at various time points and biodistribution of *Nanosota-1C-Fc* was  
229 quantified by scintillation counter. After three days, *Nanosota-1C-Fc* remained at high  
230 levels in the blood, lung, heart, kidney, liver and spleen, all of which are targets for  
231 SARS-CoV-2 (27); moreover, it remained at low levels in the intestine, muscle and  
232 bones. In contrast, *Nanosota-1C* had poor biodistribution documenting high renal  
233 clearance (Fig. S8B). Overall, our findings suggest that *Nanosota-1C-Fc* is potent SARS-  
234 CoV-2 therapeutic with translational values applicable to the world's vast population.

235

## 236 **Discussion**

237 Nanobody therapeutics derived from camelid antibodies potentially offer a  
238 realistic solution to the COVID-19 pandemic compared to conventional antibodies.  
239 Currently, there have only been a few reports of nanobody drugs that specifically target

240 SARS-CoV-2 (12, 13). Those reported were developed against SARS-CoV-2 RBD,  
241 either blocking out ACE2 or locking the RBD in the closed inactive state on the spike  
242 protein (12, 13). None of the nanobodies have been evaluated in animal models for their  
243 anti-SARS-CoV-2 therapeutic efficacy. From our novel library, we developed a series of  
244 nanobody drugs, named *Nanosota-1*, that specifically target the SARS-CoV-2 RBD. Two  
245 rounds of affinity maturation yielded *Nanosota-1C* which bound to the RBD with high  
246 affinity. Addition of an Fc tag to make a bivalent construct with increased molecular  
247 weight and picomolar RBD-binding affinity resulted in the best performing drug  
248 *Nanosota-1C-Fc*. Our structural and biochemical data showed that binding of *Nanosota-1C*  
249 to the RBD blocked virus binding to viral receptor ACE2. A unique feature of the  
250 SARS-CoV-2 spike protein is that it is present in two different conformations, an RBD-  
251 up open conformation for receptor binding and an RBD-down closed conformation for  
252 immune evasion (20, 22, 23). Due to its small size as well as its ideal binding site on the  
253 RBD, *Nanosota-1* can bind to the spike protein in both conformations. In contrast, ACE2  
254 can only bind to the spike protein in its open conformation. Thus, *Nanosota-1* drugs are  
255 ideal RBD-targeting therapeutics - they can chase down and inhibit SARS-CoV-2 viral  
256 particles whether they are infecting cells or hiding from immune surveillance. As a result  
257 of this unique property, both *Nanosota-1C* and *Nanosota-1C-Fc* exhibited a profound  
258 therapeutic effect *in vitro* against SARS-CoV-2 pseudovirus and authentic SARS-CoV-2.  
259 *Nanosota-1C-Fc* was also found to be the first anti-SARS-CoV-2 camelid nanobody-  
260 based therapeutic reported in the literature to demonstrate efficacy in an animal model.  
261 Additionally, *Nanosota-1C-Fc* was the first anti-SARS-CoV-2 nanobody to have been  
262 characterized for ease of production and purification, *in vitro* and *in vivo* stabilities, and

263 biodistribution. These features are critical for the implementation of *Nanosota-1C-Fc* as a  
264 COVID-19 therapeutic.

265 When evaluating the anti-SARS-CoV-2 potency of the nanobody therapeutics, we  
266 used recombinant ACE2 as a comparison. Recombinant ACE2 was selected because  
267 *Nanosota-1* series directly compete with cell-surface ACE2 for the same binding site on  
268 the RBD. Our study showed that compared with ACE2, the best performing drug  
269 *Nanosota-1C-Fc* bound to the RBD ~3000 fold more strongly, blocking out ACE2  
270 binding to the RBD. Furthermore, compared with ACE2, *Nanosota-1C-Fc* inhibited  
271 SARS-CoV-2 pseudovirus entry ~100 fold more effectively and inhibited authentic  
272 SARS-CoV-2 infections ~6000 fold more effectively. Note that recombinant ACE2 has  
273 been shown to be a potent anti-SARS-CoV-2 inhibitor (28) and is currently undergoing  
274 clinical trials in Europe as an anti-COVID-19 drug. Compared with ACE2, the much  
275 higher anti-SARS-CoV-2 potency of *Nanosota-1C-Fc* was due to both its much higher  
276 RBD-binding affinity and its better access to the oft-hidden RBD in the spike protein. As  
277 a result, *Nanosota-1C-Fc* was a potent therapeutic *in vivo*. Remarkably, a single dose of  
278 *Nanosota-1C-Fc* effectively prevented SARS-CoV-2 infection in hamsters and also  
279 effectively treated SARS-CoV-2 infection in the same model. The hamster model is one  
280 of the best non-primate models available for studying anti-SARS-CoV-2 therapeutic  
281 efficacy, but it is limited by a short virus infection window; hence, repeated dosing was  
282 not evaluated. As a result, we were only able to dose the mice once via intraperitoneal  
283 injection. Because SARS-CoV-2 is fast acting in hamsters, the time points and dosages  
284 for drug administration in hamsters are difficult to directly translate to humans. Our  
285 supporting data document that *Nanosota-1c-Fc* is easy to produce in bacteria and has

286 excellent bioavailability and pharmacokinetics when administered intravenously in mice.  
287 This suggests that *Nanosota-1C-Fc* may have therapeutic potential when administered  
288 intraperitoneal, intravenous or even intramuscular. These parameters will need to be  
289 determined in future studies in anticipation of clinical trials. Overall, *Nanosota-1C-Fc*  
290 has proven to be an effective therapeutic in the model that we currently have available.

291 How can the novel nanobody therapeutics help to end the COVID-19 pandemic?

292 First, as evidence by our animal study, *Nanosota-1C-Fc* can be used to prevent SARS-  
293 CoV-2 infection. Because of its long *in vivo* half-life (>10 days), a single injected dose of  
294 *Nanosota-1C-Fc* can theoretically protect a person from SARS-CoV-2 infection for days  
295 or weeks in the outpatient setting, reducing the spread of SARS-CoV-2 in human  
296 populations. Second, we also learned from our *in vivo* study that *Nanosota-1C-Fc* can  
297 potentially be used to treat SARS-CoV-2 infections, thus, saving lives and alleviating  
298 symptoms in infected patients in the clinical setting. Third, though ephemeral in nature  
299 given its short half-life and rapid clearance from the blood, *Nanosota-1C* could be used  
300 as an inhaler to treat infections in the respiratory tracts (10) or as an oral drug to treat  
301 infections in the intestines (11). Overall, the novel series of *Nanosota-1* therapeutics can  
302 help minimize the mortality and morbidity of SARS-CoV-2 infections and help restore  
303 the economy and daily human activities. Given the wide distribution of SARS-CoV-2 in  
304 the world, large quantities of anti-SARS-CoV-2 therapeutics would need to be  
305 manufactured to provide for the world's populations. This is only feasible with easy to  
306 produce and scalable molecules, such as *Nanosota-1* drugs, that are produced at high  
307 yields and have long *in vitro* and *in vivo* half-life. Therefore, if further validated in  
308 clinical trials, *Nanosota-1* therapeutics can provide a realistic and effective solution to

309 help end the COVID-19 global pandemic.

310 **Acknowledgements**

311 The development of *Nanosota-1* drugs and the animal testing were supported by  
312 funding from the University of Minnesota (to F.L.), NIH grants R01AI157975 (to F.L.,  
313 A.M.L., L.D., S.P.), R01AI089728 (to F.L.), and R35GM118047 (to H.A.). A.M.L. is a  
314 2013 Prostate Cancer Foundation Young Investigator and recipient of a 2018 Prostate  
315 Cancer Foundation Challenge Award. Experimental Pathology Laboratories analyzed  
316 pathology data on SARS-CoV-2-challenged hamsters. Crystallization screening was  
317 performed at Hauptman-Woodward Medical Research Institute and supported by NSF  
318 grant 2029943. X-ray diffraction data were collected at Advanced Photon Source  
319 beamline 24-ID-E and we thank Surajit Bannerjee for help in X-ray data collection. The  
320 University of Minnesota has filed a patent on Nanosota-1 drugs with F.L, G.Y., A.M.L.,  
321 J.P.G., J.S., and Y.W. as inventors. We thank Professor Yuhong Jiang for consultation on  
322 the design of animal testing and statistical analysis and for editing the manuscript.  
323 Coordinates and structure factors have been deposited to the Protein Data Bank with  
324 accession number XXXX.

325 **Methods**

326 *Ethics statement*

327 This study was performed in strict accordance with the recommendations in the  
328 Guide for the Care and Use of Laboratory Animals of the National Institutes of Health.  
329 All of the animals were handled according to approved institutional animal care and use  
330 committee (IACUC) protocols of the University of Texas Medical Branch (protocol  
331 number 2007072) and of the University of Minnesota (protocol number 2009-38426A).

332

333 *Cell lines, plasmids and virus*

334 HEK293T cells (American Type Culture Collection) were cultured in Dulbecco's  
335 modified Eagle medium (DMEM) supplemented with 10% fetal bovine serum, 2 mM L-  
336 glutamine, 100 units/mL penicillin, and 100 µg/mL streptomycin (Life Technologies).  
337 ss320 *E. coli* (Lucigen), TG1 *E. coli* (Lucigen), SHuffle T7 *E. coli* (New England  
338 Biolabs) were grown in TB medium or 2YT medium with 100 mg/L ampicillin. Vero E6  
339 cells (American Type Culture Collection) were grown in Eagle's minimal essential  
340 medium (EMEM) supplemented with penicillin (100 units/ml), streptomycin (100  
341 µg/ml), and 10% fetal bovine serum (FBS). SARS-CoV-2 spike (GenBank accession  
342 number QHD43416.1) and ACE2 (GenBank accession number NM\_021804) were  
343 described previously (20). SARS-CoV-2 RBD (residues 319-529) was subcloned into  
344 Lenti-CMV vector (Vigene Biosciences) with an N-terminal tissue plasminogen activator  
345 (tPA) signal peptide and a C-terminal human IgG4 Fc tag or His tag. The ACE2  
346 ectodomain (residues 1-615) was constructed in the same way except that its own signal  
347 peptide was used. *Nanosota-1A*, *-1B* and *-1C* were each cloned into PADL22c vector

348 (Lucigen) with a N-terminal PelB leader sequence and C-terminal His tag and HA tag.  
349 *Nanosota-1C-Fc* was cloned into pET42b vector (Novagen) with a C-terminal human  
350 IgG<sub>1</sub> Fc tag. SARS-CoV-2 (US\_WA-1 isolate) from CDC (Atlanta) was used throughout  
351 the study. All experiments involving infectious SARS-CoV-2 were conducted at the  
352 University of Texas Medical Branch and University of Iowa in approved biosafety level 3  
353 laboratories.

354

355 *Construction of camelid nanobody phage display library*

356 The camelid nanobody phage display library was constructed as previously  
357 described (29, 30). Briefly, total mRNA was isolated from B cells from the spleen, bone  
358 marrow and blood of over a dozen non-immunized llamas and alpacas. cDNA was  
359 prepared from the mRNA. The cDNA was then used in nested PCR reactions to construct  
360 the DNA for the library. The first PCR reaction was to amplify the gene fragments  
361 encoding the variable domain of the nanobody. The second PCR reaction (PCR2) was  
362 used to add restriction sites (SFI-I), a PelB leader sequence, a His<sub>6</sub> tag, and a HA tag. The  
363 PCR2 product was digested with SFI-I (New England Biolabs) and then was ligated with  
364 SFI-I-digested PADL22c vector. The ligated product was transformed via electroporation  
365 into TG1 *E. coli* (Lucigen). Aliquots of cells were spread onto 2YT agar plates  
366 supplemented with ampicillin and glucose, incubated at 30°C overnight, and then scraped  
367 into 2YT media. After centrifugation, the cell pellet was suspended into 50% glycerol  
368 and stored at -80°C. The library size was 7. 5 × 10<sup>10</sup>. To display nanobodies on phages,  
369 aliquots of the TG1 *E. coli* bank were inoculated into 2YT media, grown to early  
370 logarithmic phase, and infected with M13K07 helper phage.

371

372 *Camelid nanobody library screening*

373 The above camelid nanobody phage display library was used in the bio-panning  
374 as previously described (31). Briefly, four rounds of panning were performed to obtain  
375 the SARS-CoV-2 RBD-targeting nanobodies with high RBD-binding affinity. The  
376 amounts of the RBD antigen used in coating the immune tubes in each round were 75 µg,  
377 50 µg, 25 µg, and 10 µg, respectively. The retained phages were eluted using 1 ml 100  
378 mM triethylamine and neutralized with 500 µl 1 M Tris-HCl pH 7.5. The eluted phages  
379 were amplified in TG1 *E. coli* and rescued with M13K07 helper phage. The eluted  
380 phages from round 4 were used to infect ss320 *E. coli*. Single colonies were picked into  
381 2YT media and nanobody expressions were induced with 1 mM IPTG. The supernatants  
382 were subjected to ELISA for selection of strong binders (described below). The strong  
383 binders were then expressed and purified (described below) and subjected to SARS-CoV-  
384 2 pseudovirus entry assay for selection of anti-SARS-CoV-2 efficacy (described below).  
385 The lead nanobody after initial screening was named *Nanosota-1A*.

386

387 *Affinity maturation*

388 Affinity maturation of *Nanosota-1A* was performed as previously described (32).  
389 Briefly, mutations were introduced into the whole gene of *Nanosota-1A* using error-prone  
390 PCR. Two rounds of error-prone PCR were performed using the GeneMorph II Random  
391 Mutagenesis Kit (Agilent Technologies). The PCR product was cloned into the PADL22c  
392 vector and transformed via electroporation into the TG1 *E. coli*. The library size was 6 x  
393 10<sup>8</sup>. Three rounds of bio-panning were performed using 25 ng, 10 ng and 2 ng RBD-Fc,

394 respectively. The strongest binder after affinity maturation was named *Nanosota-1B*. A  
395 second round of affinity maturation was performed in the same way as the first round,  
396 except that three rounds of bio-panning were performed using 10 ng, 2 ng and 0.5 ng  
397 RBD-Fc, respectively. The strongest binder after the second round of affinity maturation  
398 was named *Nanosota-1C*.

399

400 *Production of Nanosota-1 drugs*

401 *Nanosota-1A, 1B and 1C* were each purified from the periplasm of ss320 *E. coli*  
402 after the cells were induced by 1 mM IPTG. The cells were collected and re-suspended in  
403 15 ml TES buffer (0.2 M Tris pH 8, 0.5 mM EDTA, 0.5 M sucrose), shaken on ice for 1  
404 hour and then incubated with 40 ml TES buffer followed by shaking on ice for another  
405 hour. The protein in the supernatant was sequentially purified using a Ni-NTA column  
406 and a Superdex200 gel filtration column (GE Healthcare) as previously described (20).

407 *Nanosota-1C-Fc* was purified from the cytoplasm of Shuffle T7 *E. coli*. The induction of  
408 protein expression was the same as above. After induction, the cells were collected, re-  
409 suspected in PBS and disrupted using Branson Digital Sonifier (Thermofisher). The  
410 protein in the supernatant was sequentially purified on protein A column and  
411 Superdex200 gel filtration column as previously described (20).

412

413 *Production of SARS-CoV-2 RBD and ACE2.*

414 HEK293T cells stably expressing SARS-CoV-2 RBD (containing a C-terminal  
415 His tag or Fc tag) or human ACE2 ectodomain (containing a C-terminal His tag) were  
416 made according to the E and F sections of the pLKO.1 Protocol from Addgene

417 (http://www.addgene.org/protocols/plko/). The proteins were secreted to cell culture  
418 media, harvested, and purified on either Ni-NTA column (for His-tagged proteins) or  
419 protein A column (for Fc-tagged protein) and then on Superdex200 gel filtration column  
420 as previously described (20).

421

422 *ELISA*

423 ELISA was performed to detect the binding between SARS-CoV-2 RBD and  
424 *Nanosota-1* drugs (either purified recombinant drugs or drugs in the mouse serum) as  
425 previously described (33). Briefly, ELISA plates were coated with recombinant SARS-  
426 CoV-2 RBD-His or RBD-Fc, and were then incubated sequentially with nanobody drugs,  
427 HRP-conjugated anti-llama antibody (1:5,000) (Sigma) or HRP-conjugated anti-human-  
428 Fc antibody (1:5,000) (Jackson ImmunoResearch). ELISA substrate (Invitrogen) was  
429 added to the plates, and the reactions were stopped with 1N H<sub>2</sub>SO<sub>4</sub>. The absorbance at  
430 450 nm (A<sub>450</sub>) was measured using a Synergy LX Multi-Mode Reader (BioTek).

431

432 *Determination of the structure of SARS-CoV-2 RBD complexed with Nanosota-1C*

433 To prepare the RBD/*Nanosota-1C* complex for crystallization, the two proteins  
434 were mixed together in solution and purified using a Superdex200 gel filtration column  
435 (GE Healthcare). The complex was concentrated to 10 mg/ml in buffer 20 mM Tris pH  
436 7.2 and 200 mM NaCl. Crystals were screened at High-Throughput Crystallization  
437 Screening Center (Hauptman-Woodward Medical Research Institute) as previously  
438 described (34), and were grown in sitting drops at room temperature over wells  
439 containing 50 mM MnCl<sub>2</sub>, 50 mM MES pH 6.0, 20% (W/V) PEG 4000. Crystals were

440    soaked briefly in 50 mM MnCl<sub>2</sub>, 50 mM MES pH 6.0, 25% (W/V) PEG 4000 and 30%  
441    ethylene glycol before being flash-frozen in liquid nitrogen. X-ray diffraction data were  
442    collected at the Advanced Photon Source beamline 24-ID-E. The structure was  
443    determined by molecular replacement using the structures of SARS-CoV-2 RBD (PDB  
444    6M0J) and another nanobody (PDB 6QX4) as the search templates. Structure data and  
445    refinement statistics are shown in Table S1.

446

447    *Surface plasmon resonance assay*

448        Surface plasmon resonance assay using a Biacore S200 system (GE Healthcare)  
449        was carried out as previously described (20). Briefly, SARS2-CoV-2 RBD-His was  
450        immobilized to a CM5 sensor chip (GE Healthcare). Serial dilutions of purified  
451        recombinant *Nanosota-1* drugs were injected at different concentrations: 320 nM – 10  
452        nM for *Nanosota-1A*; 80 nM - 2.5 nM for *Nanosota-1B* and *Nanosota-1C*; 20 nM - 1.25  
453        nM for *Nanosota-1C-Fc*. The resulting data were fit to a 1:1 binding model using Biacore  
454        Evaluation Software (GE Healthcare).

455

456    *Protein pull-down assay*

457        Protein pull-down assay was performed using Immunoprecipitation kit  
458        (Invitrogen) as previously described (20). Briefly, 10 µl protein A beads were incubated  
459        with 1 µg SARS-CoV-2 RBD-Fc at room temperature for 1 hour. Then different amounts  
460        (7.04, 3.52, 1.76, 0.88, 0.44, 0.22, or 0 µg) of *Nanosota-1C* (with a C-terminal His tag)  
461        and 4 µg human ACE2 (with a C-terminal His tag) were added to the RBD-bound beads.  
462        After one-hour incubation at room temperature, the bound proteins were eluted using

463 elution buffer (0.1 M glycine pH 2.7). The samples were then subjected to SDS-PAGE  
464 and analyzed through Western blot using an anti-His antibody.

465

466 *Gel filtration chromatography assay*

467 Gel filtration chromatography assay was performed on a Superdex200 column.  
468 500 µg human ACE2, 109 µg *Nanosota-1C* and 121 µg SARS-CoV-2 RBD were  
469 incubated together at room temperature for 30 min. The mixture was subjected to gel  
470 filtration chromatography. Samples from each peak off the column were then subjected to  
471 SDS-PAGE and analyzed through Coomassie blue staining.

472

473 *SARS-CoV-2 pseudovirus entry assay*

474 The potency of *Nanosota-1* drugs in neutralizing SARS-CoV-2 pseudovirus entry  
475 was evaluated as previously described (20, 22). Briefly, HEK293T cells were co-  
476 transfected with a plasmid carrying an Env-defective, luciferase-expressing HIV-1  
477 genome (pNL4-3.luc.R-E-) and pcDNA3.1(+) plasmid encoding SARS-CoV-2 spike  
478 protein. Pseudoviruses were collected 72 hours after transfection, incubated with  
479 individual drugs at different concentrations at 37°C for one hour, and then were used to  
480 enter HEK293T cells expressing human ACE2. After pseudoviruses and target cells were  
481 incubated together at 37°C for 6 hours, the medium was changed to fresh medium,  
482 followed by incubation of another 60 hours. Cells were then washed with PBS buffer and  
483 lysed. Aliquots of cell lysates were transferred to plates, followed by the addition of  
484 luciferase substrate. Relative light units (RLUs) were measured using an EnSpire plate

485 reader (PerkinElmer). The efficacy of the drug was expressed as the concentration  
486 capable of neutralizing 50% of the entry efficiency (Neutralizing Dose 50 or ND<sub>50</sub>).

487

488 *SARS-CoV-2 plaque reduction neutralization test*

489 The potency of *Nanosota-1* drugs in neutralizing authentic SARS-CoV-2  
490 infections was evaluated using a SARS-CoV-2 plaque reduction neutralization test  
491 (PRNT) assay. Specifically, individual drugs were serially diluted in DMEM and mixed  
492 1:1 with 80 pfu SARS-CoV-2 at 37°C for 1 hour. The mixtures were then added into  
493 Vero E6 cells at 37°C for an additional 45 minutes. After removing the culture medium,  
494 cells were overlaid with 0.6% agarose and cultured for 3 days. Plaques were visualized  
495 by 0.1% crystal violet staining. The efficacy of each drug was calculated and expressed  
496 as the concentration capable of reducing the number of virus plaques by 50% compared  
497 to control serum-exposed virus (i.e., ND<sub>50</sub>).

498

499 *SARS-CoV-2 challenge of hamsters*

500 Equal sex Syrian hamsters (n=24) were obtained from Envigo (IN) and  
501 challenged via intranasal inoculation with SARS-CoV-2 (at a titer of 1 x 10<sup>6</sup> Median  
502 Tissue Culture Infectious Dose or TCID<sub>50</sub>) in 100 µL DMEM (50 µL per nare). Sample  
503 size was comparable to previous animal challenge studies (33) and constrained by the  
504 availability of resources. At a sample size of 6 animals per group, G\*Power analysis  
505 indicates that we can detect an effect size of 1.6 with a power of .80 (alpha = .05 one-  
506 tailed). Four groups of hamsters (n=6 each randomly assigned) were treated with  
507 *Nanosota-1C-Fc* via intraperitoneal injection at one of the following time points and

508 dosages: (1) 24 hours pre-challenge at 20 mg/kg body weight of hamsters; (2) 4 hours  
509 post-challenge at 20 mg/kg body weight of hamsters; (3) 4 hours post-challenge at 10  
510 mg/kg body weight of hamsters. Hamsters in the control (negative) group were  
511 administered PBS buffer 24 hours pre-challenge. An additional group was tested for a  
512 different hypothesis and the data were not included in the current study. Body weights  
513 were collected daily beginning prior to challenge. Nasal swabs were collected prior to  
514 challenge and additionally 1 day, 2 days, 3 days, 5 days and 10 days post-challenge for  
515 quantitative real-time RT-PCR (nasal swabs collected on day 2 and day 3 were lost due to  
516 Hurricane Laura). Hamsters were humanely euthanized 10 days post-challenge via  
517 overexposure to CO<sub>2</sub>. The lungs and bronchial tubes were collected and fixed in formalin  
518 for histopathological analysis. This experiment was performed in accordance with the  
519 guidelines set by the Institutional Animal Care and Use Committee at the University of  
520 Texas Medical Branch (UTMB).

521

522 *Half-life of Nanosota-1 drugs in mice*

523 Male C57BL/6 mice (3 to 4 weeks old) (Envigo) were intravenously injected (tail-  
524 vein) with *Nanosota-1C* or *Nanosota-1C-Fc* (100 µg in 100 µl PBS buffer). At varying  
525 time points, mice were euthanized and whole blood was collected. Then sera were  
526 prepared through centrifugation of the whole blood at 1500xg for 10 min. The sera were  
527 then subjected to ELISA for evaluation of their SARS-CoV-2 RBD-binding capability.

528

529 *Biodistribution of Nanosota-1 drugs in mice*

530 To evaluate the *in vivo* biodistribution of *Nanosota-1C-Fc* and *Nanosota-1C*, the  
531 nanobodies were labeled with Zirconium-89 [<sup>89</sup>Zr] and injected into male C57BL/6 mice  
532 (5 to 6 weeks old) (Envigo). Briefly, the nanobodies were first conjugated to the  
533 bifunctional chelator p-SCN-Bn-Deferoxamine (DFO, Macroyclic) as previously  
534 described (35), and [<sup>89</sup>Zr] (University of Wisconsin Medical Physics Department) was  
535 then conjugated as previously described (36). [<sup>89</sup>Zr]-labeled nanobodies (1.05 MBq, 1-2  
536 µg nanobody, 100 µl PBS) were intravenously injected (tail-vein). Mice were euthanized  
537 at different time points. Organs were collected and counted on an automatic gamma-  
538 counter (Hidex). The total number of counts per minute (cpm) for each organ or tissue  
539 was compared with a standard sample of known activity and mass. Count data were  
540 corrected to both background and decay. The percent injected dose per gram (%ID/g) was  
541 calculated by normalization to the total amount of activity injected into each mouse.

542

543 **References**

544

545 1. Q. Li *et al.*, Early Transmission Dynamics in Wuhan, China, of Novel  
546 Coronavirus-Infected Pneumonia. *N Engl J Med*, (2020).

547 2. C. Huang *et al.*, Clinical features of patients infected with 2019 novel coronavirus  
548 in Wuhan, China. *Lancet*, (2020).

549 3. G. Salazar, N. Zhang, T. M. Fu, Z. An, Antibody therapies for the prevention and  
550 treatment of viral infections. *NPJ vaccines* **2**, 19 (2017).

551 4. F. C. Breedveld, Therapeutic monoclonal antibodies. *Lancet* **355**, 735-740 (2000).

552 5. D. Könning *et al.*, Camelid and shark single domain antibodies: structural features  
553 and therapeutic potential. *Curr Opin Struct Biol* **45**, 10-16 (2017).

554 6. T. De Meyer, S. Muyldermans, A. Depicker, Nanobody-based products as  
555 research and diagnostic tools. *Trends Biotechnol* **32**, 263-270 (2014).

556 7. S. Muyldermans, Nanobodies: natural single-domain antibodies. *Annu Rev*  
557 *Biochem* **82**, 775-797 (2013).

558 8. S. Steeland, R. E. Vandebroucke, C. Libert, Nanobodies as therapeutics: big  
559 opportunities for small antibodies. *Drug discovery today* **21**, 1076-1113 (2016).

560 9. M. Scully *et al.*, Caplacizumab Treatment for Acquired Thrombotic  
561 Thrombocytopenic Purpura. *N Engl J Med* **380**, 335-346 (2019).

562 10. G. Van Heeke *et al.*, Nanobodies® as inhaled biotherapeutics for lung diseases.  
563 *Pharmacology & therapeutics* **169**, 47-56 (2017).

564 11. C. G. Vega *et al.*, Recombinant monovalent llama-derived antibody fragments  
565 (VHH) to rotavirus VP6 protect neonatal gnotobiotic piglets against human  
566 rotavirus-induced diarrhea. *PLoS Pathog* **9**, e1003334 (2013).

567 12. J. Huo *et al.*, Neutralizing nanobodies bind SARS-CoV-2 spike RBD and block  
568 interaction with ACE2. *Nat Struct Mol Biol*, (2020).

569 13. M. Schoof *et al.*, An ultra-potent synthetic nanobody neutralizes SARS-CoV-2 by  
570 locking Spike into an inactive conformation. *bioRxiv*, 2020.2008.2008.238469  
571 (2020).

572 14. F. Li, Receptor recognition mechanisms of coronaviruses: a decade of structural  
573 studies. *J Virol* **89**, 1954-1964 (2015).

574 15. F. Li, Structure, Function, and Evolution of Coronavirus Spike Proteins. *Annual*  
575 *review of virology* **3**, 237-261 (2016).

576 16. S. Perlman, J. Netland, Coronaviruses post-SARS: update on replication and  
577 pathogenesis. *Nature Reviews Microbiology* **7**, 439-450 (2009).

578 17. Y. Wan, J. Shang, R. Graham, R. S. Baric, F. Li, Receptor Recognition by the  
579 Novel Coronavirus from Wuhan: an Analysis Based on Decade-Long Structural  
580 Studies of SARS Coronavirus. *J Virol* **94**, (2020).

581 18. W. H. Li *et al.*, Angiotensin-converting enzyme 2 is a functional receptor for the  
582 SARS coronavirus. *Nature* **426**, 450-454 (2003).

583 19. P. Zhou *et al.*, A pneumonia outbreak associated with a new coronavirus of  
584 probable bat origin. *Nature*, (2020).

585 20. J. Shang *et al.*, Structural basis of receptor recognition by SARS-CoV-2. *Nature*  
586 **581**, 221-224 (2020).

587 21. F. Li, W. H. Li, M. Farzan, S. C. Harrison, Structure of SARS coronavirus spike  
588 receptor-binding domain complexed with receptor. *Science* **309**, 1864-1868  
589 (2005).

590 22. J. Shang *et al.*, Cell entry mechanisms of SARS-CoV-2. *Proc Natl Acad Sci U S A*  
591 **117**, 11727-11734 (2020).

592 23. D. Wrapp *et al.*, Cryo-EM structure of the 2019-nCoV spike in the prefusion  
593 conformation. *Science*, (2020).

594 24. Z. Ke *et al.*, Structures and distributions of SARS-CoV-2 spike proteins on intact  
595 virions. *Nature*, (2020).

596 25. B. Korber *et al.*, Tracking Changes in SARS-CoV-2 Spike: Evidence that D614G  
597 Increases Infectivity of the COVID-19 Virus. *Cell* **182**, 812-827.e819 (2020).

598 26. S. F. Sia *et al.*, Pathogenesis and transmission of SARS-CoV-2 in golden  
599 hamsters. *Nature* **583**, 834-838 (2020).

600 27. V. G. Puelles *et al.*, Multiorgan and Renal Tropism of SARS-CoV-2. *N Engl J  
601 Med* **383**, 590-592 (2020).

602 28. K. H. Monteil V, Prado P, et al. , Inhibition of SARS-CoV-2 infections in  
603 engineered human tissues using clinical-grade soluble human ACE2. *Cell*,  
604 (2020).

605 29. A. Q. Abbady, A. Al-Mariri, M. Zarkawi, A. Al-Assad, S. Muyldermans,  
606 Evaluation of a nanobody phage display library constructed from a Brucella-  
607 immunised camel. *Veterinary immunology and immunopathology* **142**, 49-56  
608 (2011).

609 30. A. Olichon, A. de Marco, Preparation of a naïve library of camelid single domain  
610 antibodies. *Methods in molecular biology* (Clifton, N.J.) **911**, 65-78 (2012).

611 31. H. M. Hintz, A. E. Cowan, M. Shapovalova, A. M. LeBeau, Development of a  
612 Cross-Reactive Monoclonal Antibody for Detecting the Tumor Stroma.  
613 *Bioconjugate chemistry* **30**, 1466-1476 (2019).

614 32. M. Hust, T. S. Lim, *Phage display : methods and protocols*. (2018).

615 33. G. Zhao *et al.*, A Novel Nanobody Targeting Middle East Respiratory Syndrome  
616 Coronavirus (MERS-CoV) Receptor-Binding Domain Has Potent Cross-  
617 Neutralizing Activity and Protective Efficacy against MERS-CoV. *J Virol* **92**,  
618 (2018).

619 34. J. R. Luft *et al.*, A deliberate approach to screening for initial crystallization  
620 conditions of biological macromolecules. *Journal of structural biology* **142**, 170-  
621 179 (2003).

622 35. B. M. Zeglis, J. S. Lewis, The bioconjugation and radiosynthesis of 89Zr-DFO-  
623 labeled antibodies. *Journal of visualized experiments : JoVE*, (2015).

624 36. H. M. Hintz *et al.*, Imaging Fibroblast Activation Protein Alpha Improves  
625 Diagnosis of Metastatic Prostate Cancer with Positron Emission Tomography.  
626 *Clinical cancer research : an official journal of the American Association for  
627 Cancer Research*, (2020).

628

629 **Table 1. Binding affinities between *Nanosota-1* drugs and SARS-CoV-2 RBD as**  
630 **measured using surface plasmon resonance.** The previously determined binding  
631 affinity between human ACE2 and RBD is shown as a comparison (20).  
632

	$K_d$ with SARS-CoV-2 RBD (M)	$k_{off}$ (s <sup>-1</sup> )	$k_{on}$ (M <sup>-1</sup> s <sup>-1</sup> )
<i>Nanosota-1A</i> (before affinity maturation)	$2.28 \times 10^{-7}$	$9.35 \times 10^{-3}$	$4.10 \times 10^4$
<i>Nanosota-1B</i> (after 1 <sup>st</sup> round of affinity maturation)	$6.08 \times 10^{-8}$	$7.19 \times 10^{-3}$	$1.18 \times 10^5$
<i>Nanosota-1C</i> (after 2 <sup>nd</sup> round of affinity maturation)	$1.42 \times 10^{-8}$	$2.96 \times 10^{-3}$	$2.09 \times 10^5$
<i>Nanosota-1C-Fc</i> (after 2 <sup>nd</sup> round of affinity maturation; containing a C-terminal human Fc tag)	$1.57 \times 10^{-11}$	$9.68 \times 10^{-5}$	$6.15 \times 10^6$
ACE2	$4.42 \times 10^{-8}$	$7.75 \times 10^{-3}$	$1.75 \times 10^5$

633  
634

635 **Figure legends:**

636 **Figure 1: Construction of a camelid nanobody phage display library and use of this**  
637 **library for screening of anti-SARS-CoV-2 nanobodies.** A large-sized (diversity 7.5 x  
638  $10^{10}$ ), naïve nanobody phage display library was constructed using B cells of over a  
639 dozen llamas and alpacas. Phages were screened for their high binding affinity for SARS-  
640 CoV-2 RBD. Nanobodies expressed from the selected phages were further screened for  
641 their potency in neutralizing SARS-CoV-2 pseudovirus entry. The best performing  
642 nanobody was subjected to two rounds of affinity maturation.

643

644 **Figure 2: Crystal structure of SARS-CoV-2 RBD complexed with *Nanosota-1C*.** (A)  
645 Structure of SARS-CoV-2 RBD complexed with *Nanosota-1C*, viewed at two different  
646 angles. *Nanosota-1C* is in red, the core structure of RBD is in cyan, and the receptor-  
647 binding motif (RBM) of RBD is in magenta. (B) Overlay of the structures of the  
648 RBD/*Nanosota-1C* complex and RBD/ACE2 complex (PDB 6M0J). ACE2 is in green.  
649 The structures of the two complexes were superimposed based on their common RBD  
650 structure. The *Nanosota-1C* loops that have clashes with ACE2 are in blue.

651

652 **Figure 3. Efficacy of *Nanosota-1* drugs in neutralizing SARS-CoV-2 infections *in***  
653 ***vitro*.** (A) Neutralization of SARS-CoV-2 pseudovirus entry into target cells by one of  
654 three inhibitors: *Nanosota-1C-Fc*, *Nanosota-1C*, and recombinant human ACE2.  
655 Retroviruses pseudotyped with SARS-CoV-2 spike protein (i.e., SARS-CoV-2  
656 pseudoviruses) were used to enter HEK293T cells expressing human ACE2 in the  
657 presence of the inhibitor at various concentrations. Entry efficiency was characterized via

658 a luciferase signal indicating successful cell entry. Data are the mean  $\pm$  SEM (n = 4).  
659 Nonlinear regression was performed using a log (inhibitor) versus normalized response  
660 curve and a variable slope model ( $R^2 > 0.95$  for all curves). The efficacy of each inhibitor  
661 was expressed as the 50% Neutralizing Dose or  $ND_{50}$ . The assay was repeated three times  
662 (biological replication: new aliquots of pseudoviruses and cells were used for each  
663 repeat). (B) Neutralization of authentic SARS-CoV-2 infection of target cells by one of  
664 two inhibitors: *Nanosota-1C-Fc* and *Nanosota-1C*. The potency of *Nanosota-1* drugs in  
665 neutralizing authentic SARS-CoV-2 infections was evaluated using a SARS-CoV-2  
666 plaque reduction neutralization test (PRNT) assay. 80 pfu infectious SARS-CoV-2  
667 particles were used to infect Vero E6 cells in the presence of the inhibitor at various  
668 concentrations. Infection was characterized as the number of virus plaques formed in  
669 overlaid cells. Images of virus plaques for each inhibitor at the indicated concentrations  
670 are shown. Each image represents data from triplications. The efficacy of each inhibitor  
671 was calculated and expressed as the concentration capable of reducing the number of  
672 virus plaques by 50% (i.e.,  $ND_{50}$ ). The assay was repeated twice (biological replication:  
673 new aliquots of virus particles and cells were used for each repeat).

674

675 **Figure 4. Efficacy of *Nanosota-1* drugs in protecting hamsters from SARS-CoV-2**  
676 **infections.** Hamsters (6 per group) were injected with a single dose of *Nanosota-1C-Fc* at  
677 the indicated time point and the indicated dosage. At day 0 all groups (experimental and  
678 control) were challenged with SARS-CoV-2 (at a titer of  $10^6$  Median Tissue Culture  
679 Infectious Dose or  $TCID_{50}$ ). (A) Body weights of hamsters were monitored on each day  
680 and percent change in body weight relative to day 0 was calculated for each hamster.

681 Data are the mean  $\pm$  SEM (n = 6). ANOVA on group as a between-group factor and day  
682 (1-10) as a within-group factor revealed significant differences between the control group  
683 and each of the following groups: 24 hour pre-challenge (20 mg/kg) group ( $F(1, 10) =$   
684 17.80,  $p = .002$ ; effect size  $\eta_p^2 = .64$ ), 4 hour post-challenge (20 mg/kg) group ( $F(1, 10) =$   
685 5.02,  $p = .035$ ;  $\eta_p^2 = .37$ ), and 4 hour post-challenge (10 mg/kg) group ( $F(1, 10) = 7.04$ ,  $p$   
686 = .024,  $\eta_p^2 = .41$ ). All  $p$ -values are two-tailed. (B) Tissues of bronchial tubes from each of  
687 the hamsters were collected on day 10 and scored for the severity of bronchioloalveolar  
688 hyperplasia: 3 - moderate; 2 - mild; 1 - minimum; 0 - none. Data are the mean  $\pm$  SEM (n  
689 = 6). A comparison between the control group and each of other groups was performed  
690 using one-tailed Student's t-test for directional tests. \*\*\* $p < 0.001$ ; \* $p < 0.05$ .

691

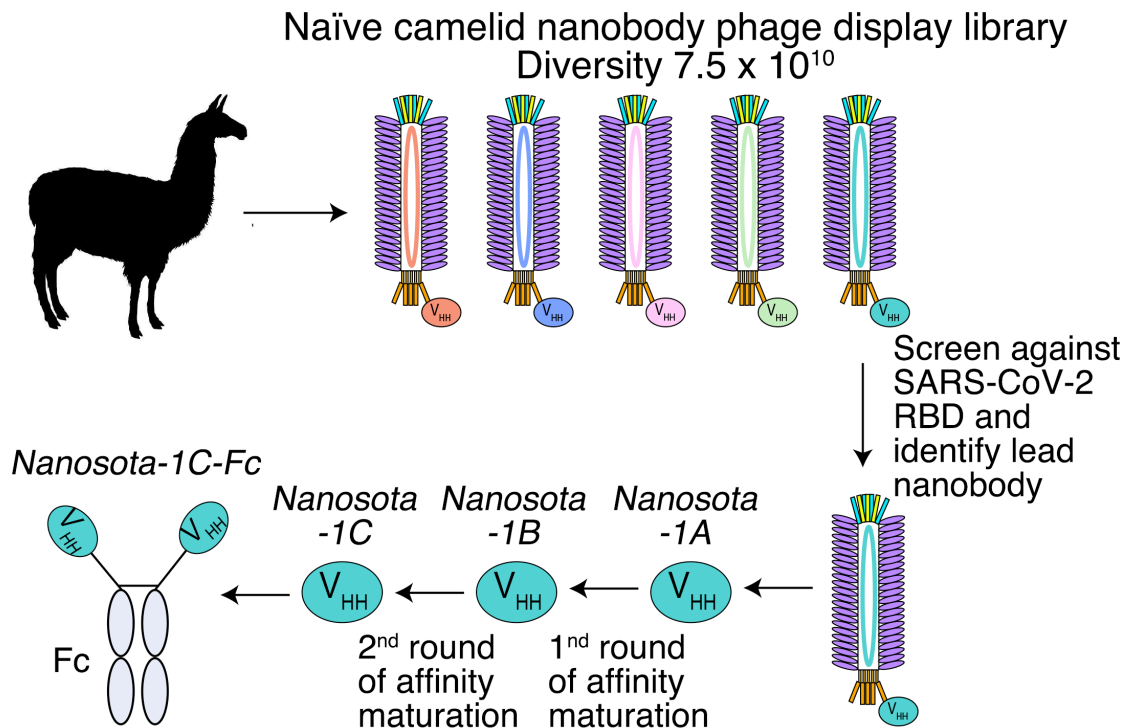
692 **Figure 5. Analysis of expression, purification and pharmacokinetics of Nanosota-1C-Fc.** (A) Purification of Nanosota-1C-Fc from bacteria. The protein was nearly 100% pure  
693 after gel filtration chromatography, as demonstrated by its elution profile and SDS-PAGE  
694 (stained by Coomassie blue). The yield of the protein was 40 mg/L of bacterial culture,  
695 without any optimization of the expression. (B) *In vitro* stability of Nanosota-1C-Fc. The  
696 protein was stored at indicated temperatures for a week, and then a dilution ELISA was  
697 performed to evaluate its SARS-CoV-2 RBD-binding capability. Data are the mean  $\pm$   
698 SEM (n = 4). (C) *In vivo* stability of Nanosota-1C-Fc. Nanosota-1C-Fc was injected into  
699 mice, mouse sera were collected at different time points, and Nanosota-1C-Fc remaining  
700 in the sera was detected for its SARS-CoV-2 RBD-binding capability as displayed in a  
701 dilution ELISA. Data are the mean  $\pm$  SEM (n = 3). (D) Biodistribution of [<sup>89</sup>Zr]Zr-  
702 Nanosota-1C-Fc. Nanosota-1C-Fc was radioactively labeled with <sup>89</sup>Zr and injected into

704 mice via tail vein injection. Different tissues or organs were collected at various time  
705 points (n=3 mice per time point). The amount of *Nanosota-1C-Fc* present in each tissue  
706 or organ was measured through examining the radioactive count of each tissue or organ.  
707 Data are the mean  $\pm$  SEM (n = 3).

708

709

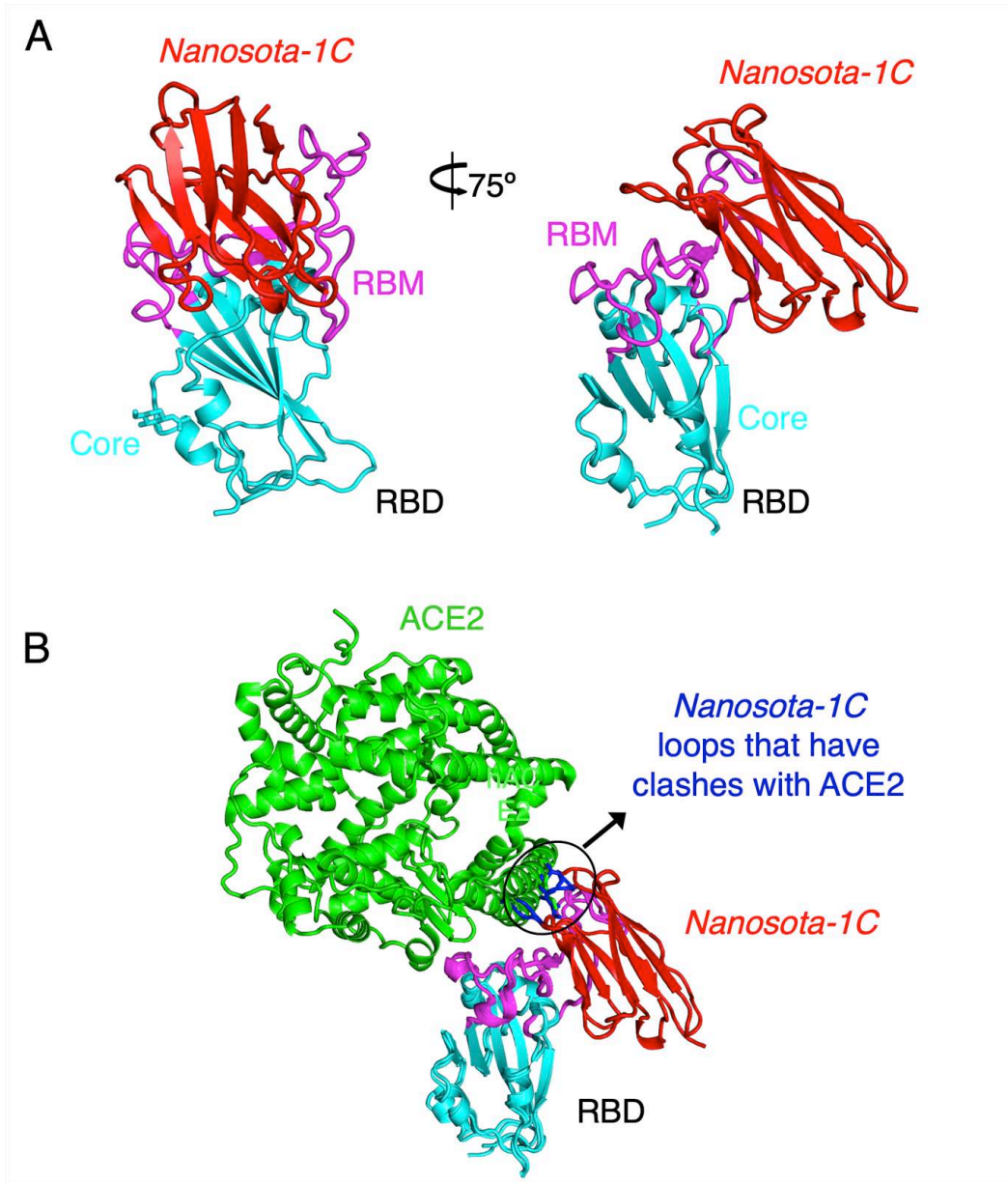
710 Figure 1



711

712

713 Figure 2

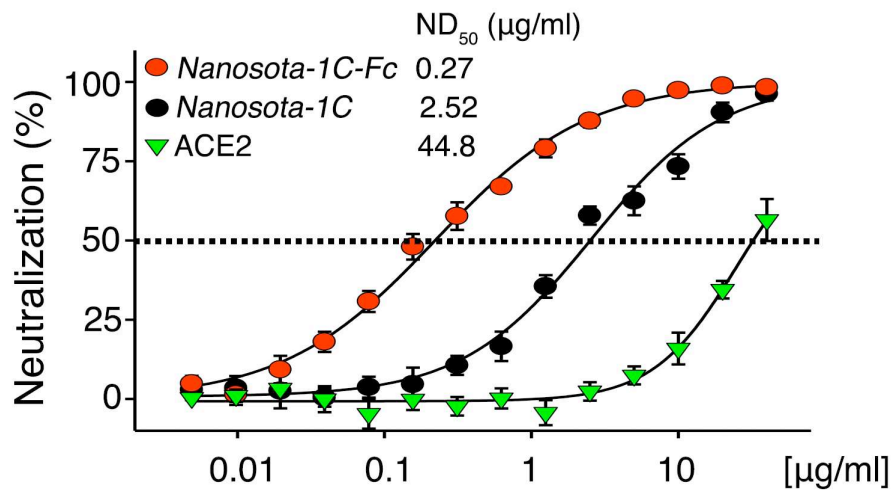


714

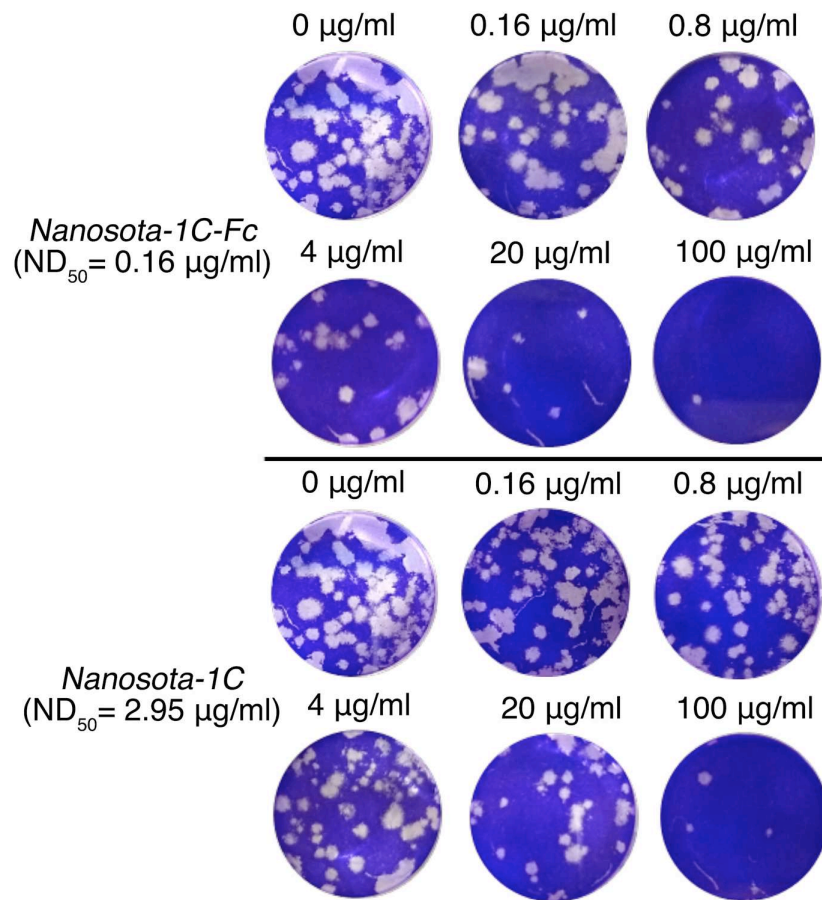
715

716 Figure 3

### A SARS-CoV-2 pseudovirus neutralization

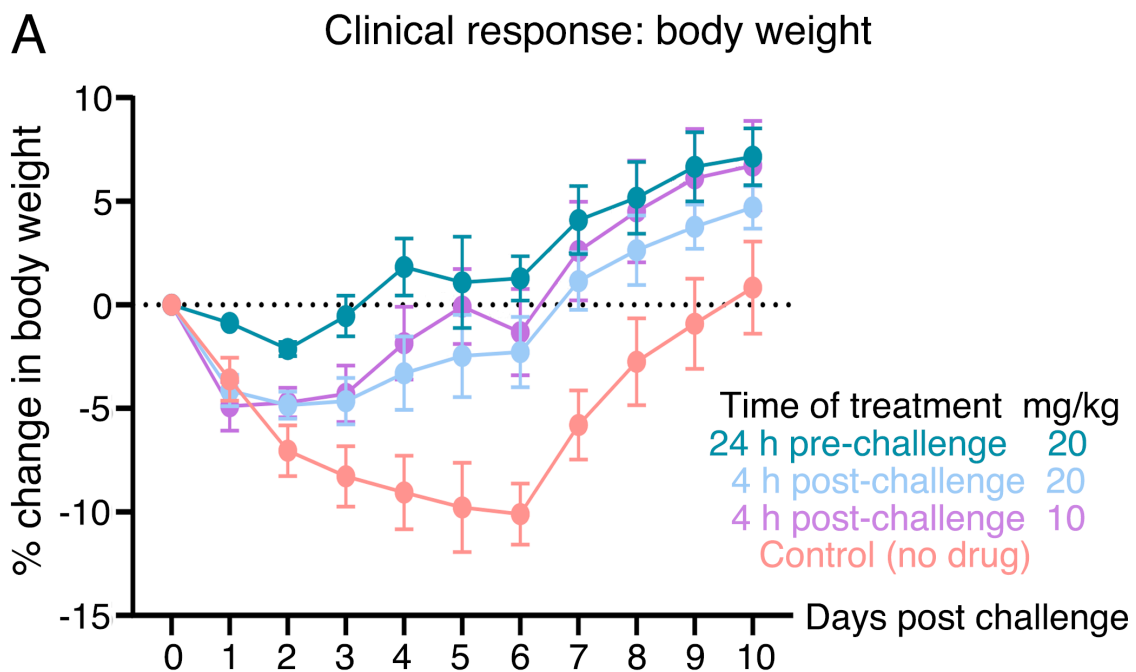


### B Authentic SARS-CoV-2 neutralization

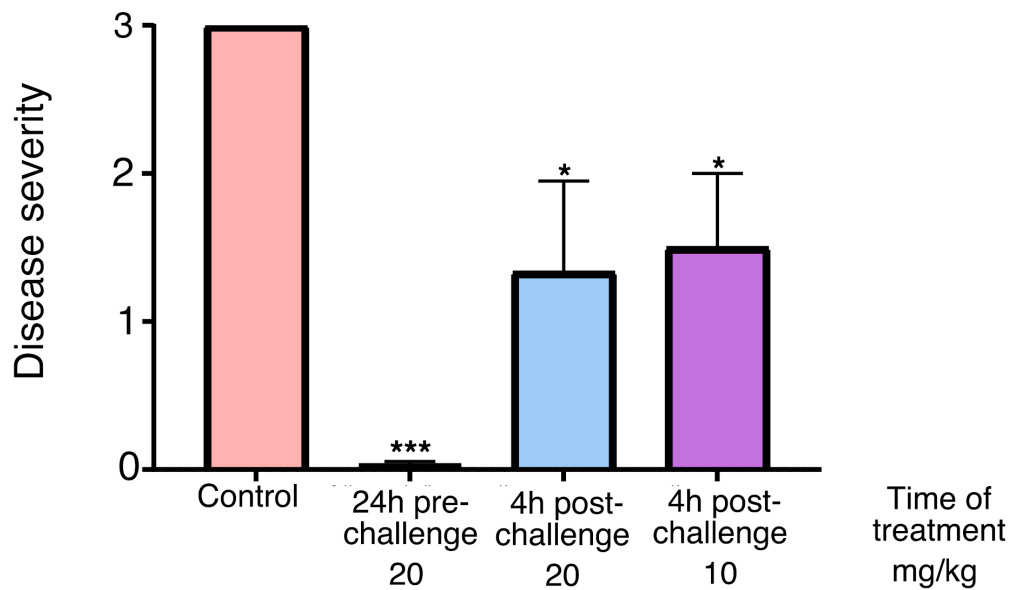


717

718 Figure 4



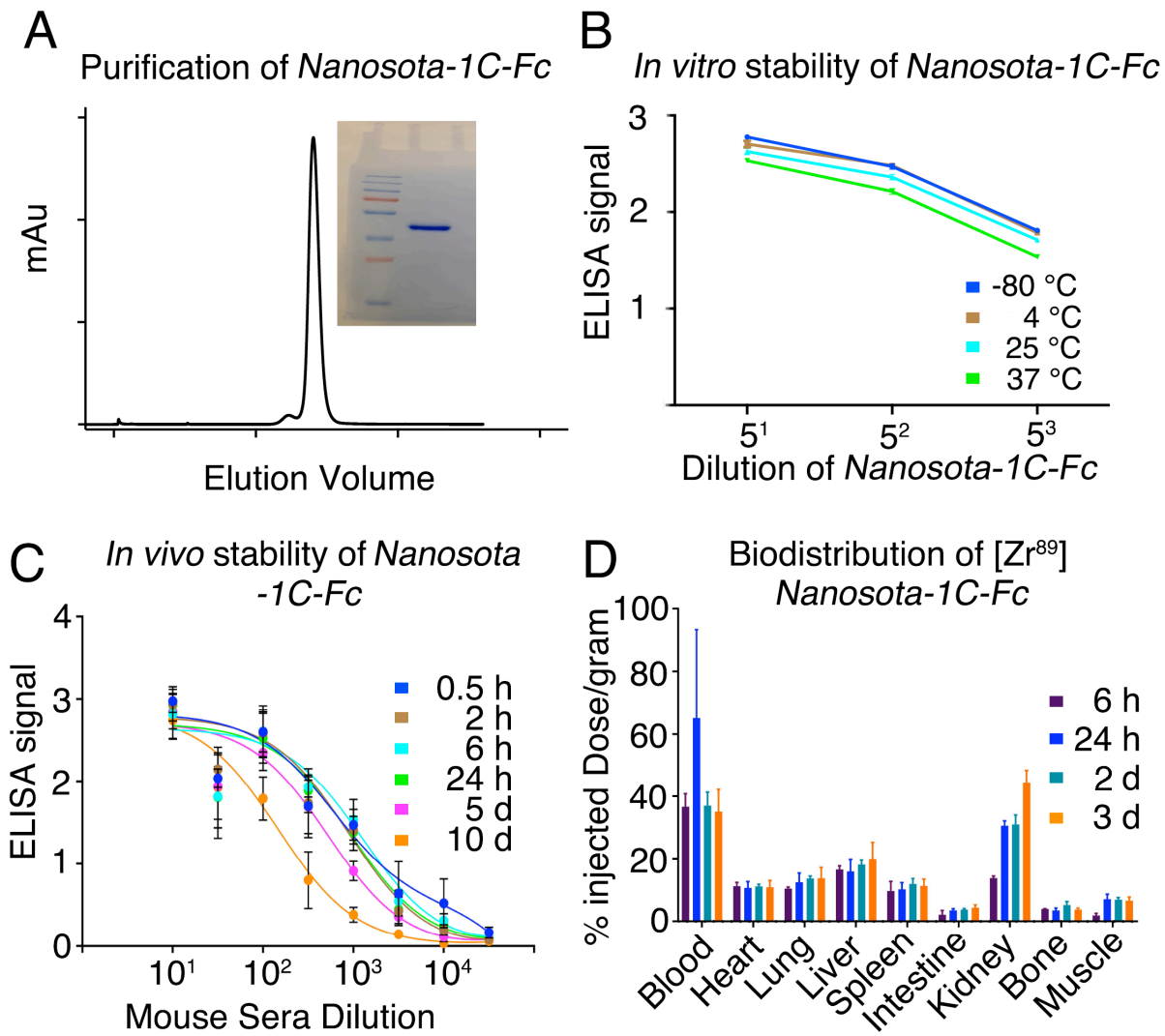
**B Pathology: bronchioloalveolar hyperplasia**



719

720

721 Figure 5



722

723

724    **Supplementary materials for**

725

726    **“The Development of a Novel Nanobody Therapeutic for SARS-CoV-2”**

727

728            Gang Ye <sup>1,\*</sup>, Joseph P. Gallant <sup>2,\*</sup>, Christopher Massey <sup>3</sup>, Ke Shi <sup>4</sup>, Wanbo Tai <sup>5</sup>,  
729            Jian Zheng <sup>6</sup>, Abby E. Odle <sup>6</sup>, Molly A. Vickers <sup>6</sup>, Jian Shang <sup>1</sup>, Yushun Wan <sup>1</sup>,  
730            Aleksandra Drellich <sup>7</sup>, Kempaiah R. Kempaiah <sup>7</sup>, Vivian Tat <sup>8</sup>, Stanley Perlman <sup>6</sup>,  
731            Lanying Du <sup>5</sup>, Chien-Te Tseng <sup>7,9</sup>, Hideki Aihara <sup>4</sup>, Aaron M. LeBeau <sup>2,#</sup>, Fang Li <sup>1,#</sup>  
732

733 **Table S1. X-ray data collection and structure refinement statistics**  
734 **(SARS-CoV-2 RBD/*Nanosota-1C* complex)**

**Data collection**

Wavelength	0.979
Resolution range	45.48 - 3.19 (3.30 - 3.19)
Space group	P 43 21 2
Unit cell	60.849 60.849 410.701 90 90 90
Total reflections	64167 (5703)
Unique reflections	13607 (1308)
Multiplicity	4.7 (4.4)
Completeness (%)	96.82 (97.60)
Mean I/sigma(I)	8.41 (1.80)
Wilson B-factor	83.24
R-merge	0.145 (0.928)
R-meas	0.1638 (1.053)
R-pim	0.07385 (0.4858)
CC1/2	0.995 (0.861)
CC*	0.999 (0.962)

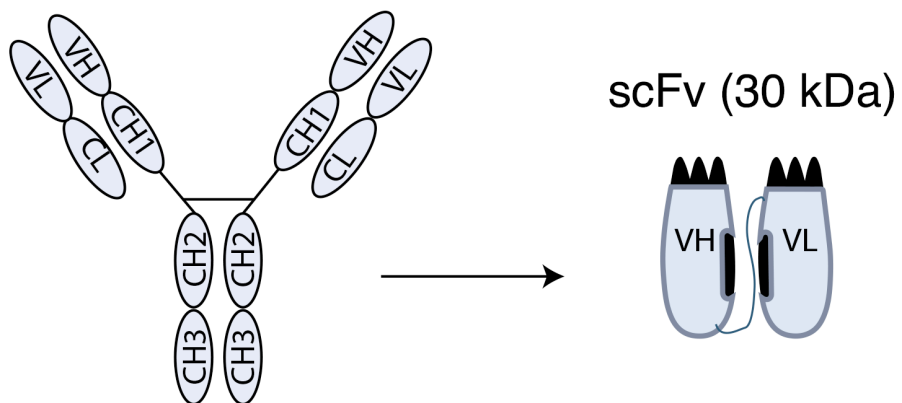
**Refinement**

Reflections used in refinement	13567 (1301)
Reflections used for R-free	674 (62)
R-work	0.2483 (0.3521)
R-free	0.2959 (0.4153)
CC(work)	0.963 (0.819)
CC(free)	0.909 (0.615)
Number of non-hydrogen atoms	4890
macromolecules	4833
ligands	57
Protein residues	621
RMS(bonds)	0.002
RMS(angles)	0.45
Ramachandran favored (%)	93.11
Ramachandran allowed (%)	6.89
Ramachandran outliers (%)	0.00
Rotamer outliers (%)	3.23
Clashscore	5.25
Average B-factor	90.29
macromolecules	89.84
ligands	127.91

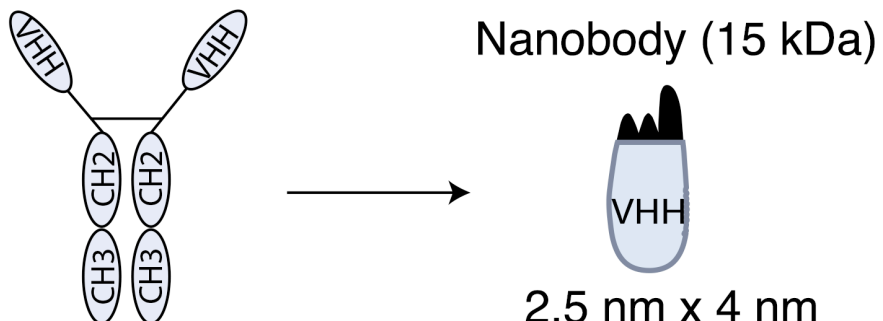
735 Statistics for the highest-resolution shell are shown in parentheses.  
736

737

## Conventional antibody (150 kDa)

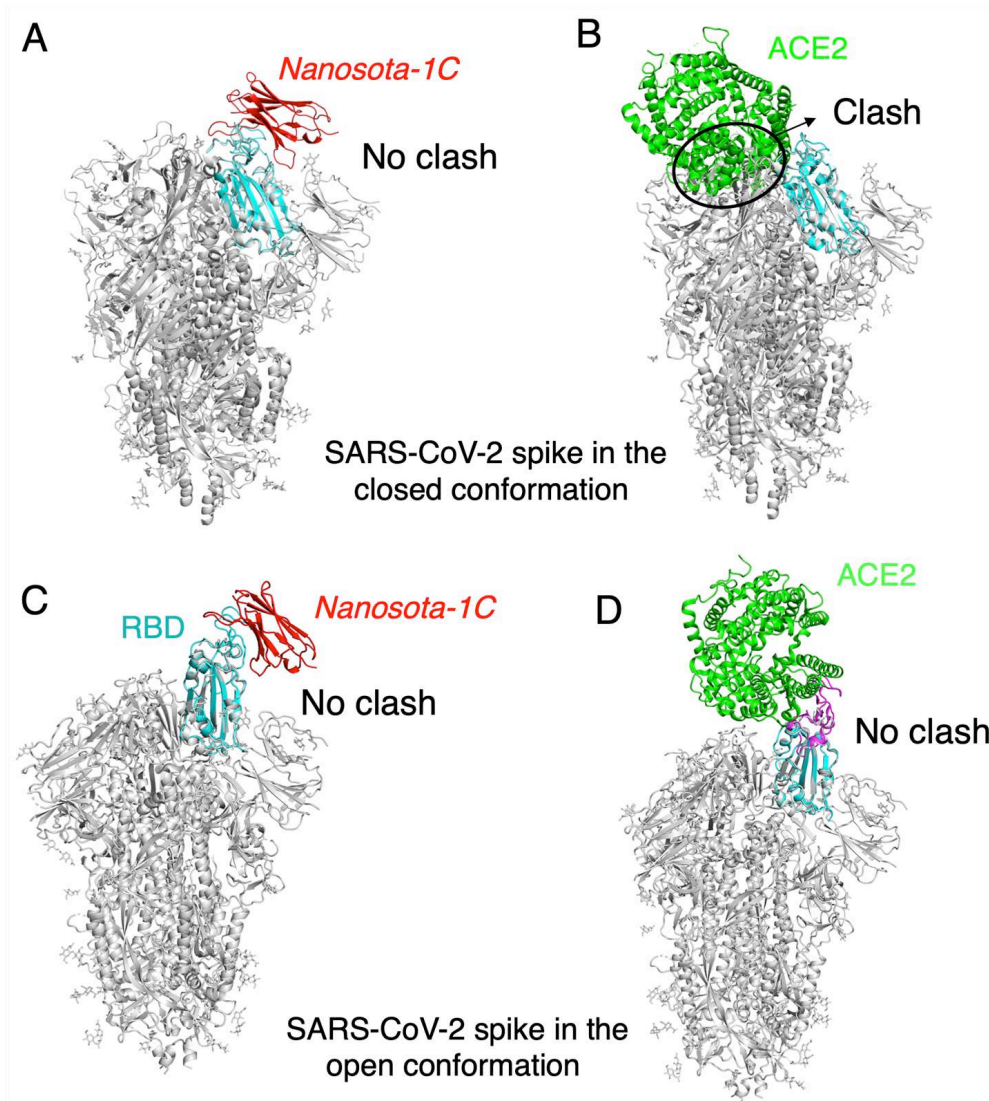


## Heavy chain only antibody (80 kDa)



738

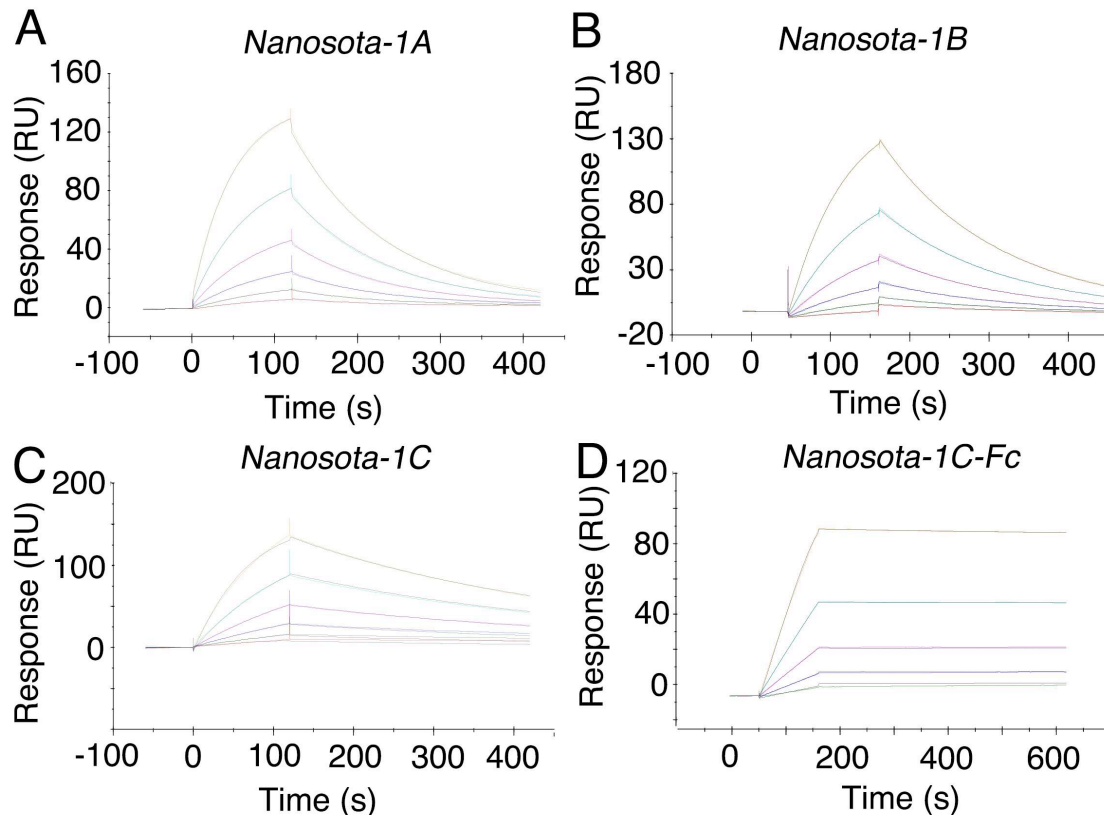
739 **Figure S1. Schematic drawings of nanobodies and conventional antibodies.** VH:  
740 variable domain of heavy chain. CH: constant domain of heavy chain. VL: variable  
741 domain of light chain. CL: constant domain of light chain. VHH: variable domain of  
742 heavy-chain only antibody. scFv: single-chain variable fragment.  
743



744  
745

746 **Figure S2. The binding of Nanosota-1C to SARS-CoV-2 spike protein in different**  
747 **conformations.** (A) The binding of Nanosota-1C to the spike protein in the closed  
748 conformation. The structures of the RBD/Nanosota-1C complex and SARS-CoV-2 spike  
749 protein in the closed conformation (PDB: 6ZWV) were superimposed based on their  
750 common RBD structure (in cyan). Nanosota-1C is in red. The rest of the spike protein is  
751 in gray. (B) The binding of ACE2 to the spike protein in the closed conformation. The  
752 structures of the RBD/ACE2 complex (PDB 6M0J) and SARS-CoV-2 spike protein in  
753 the closed conformation (PDB: 6ZWV) were superimposed based on their common RBD  
754 structure. ACE2 is in green. Clashes between ACE2 and the rest of the spike protein were  
755 circled. (C) The binding of Nanosota-1C to the spike protein in the open conformation  
756 (PDB: 6VSB). (D) The binding of ACE2 to the spike protein in the open conformation  
757 (PDB: 6VSB).

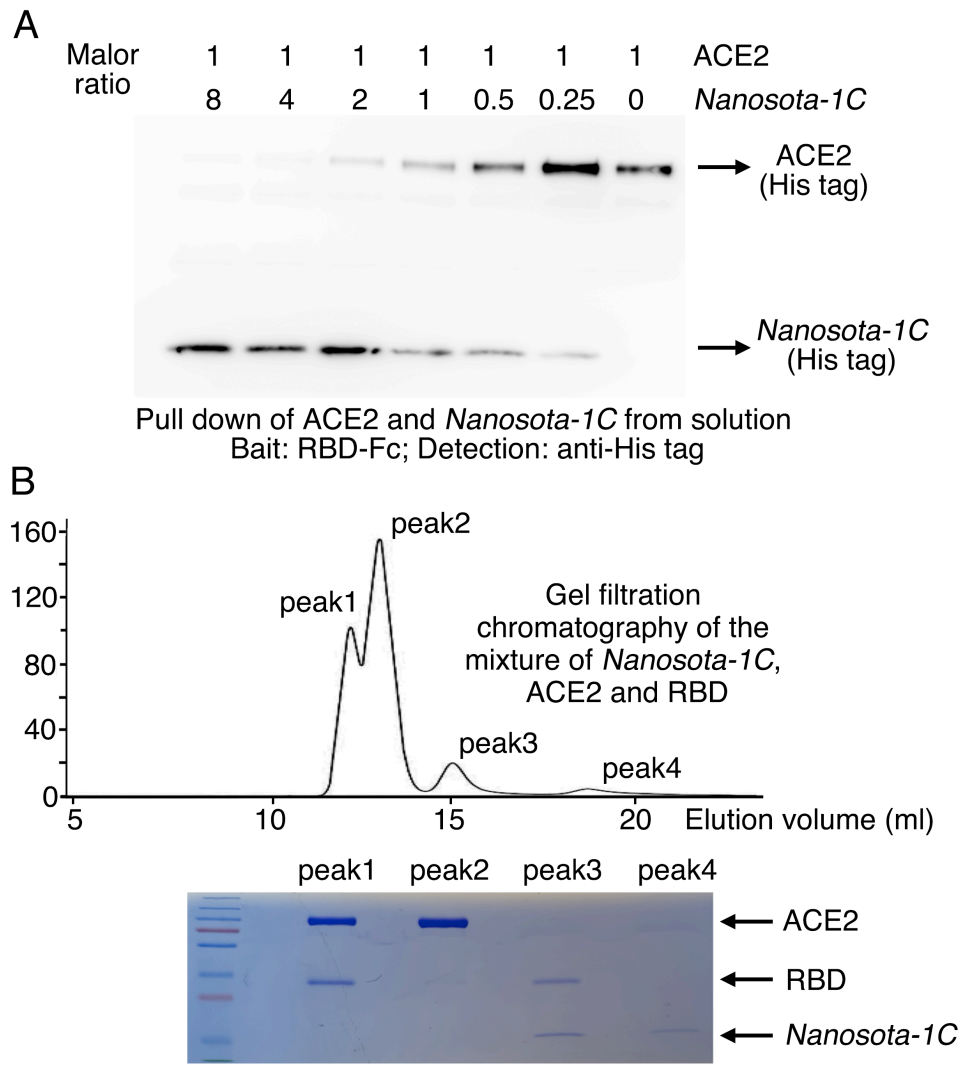
758



759

760 **Figure S3. Measurement of the binding affinities between *Nanosota-1* drugs and**  
761 **SARS-CoV-2 RBD by surface plasmon resonance assay using Biacore.** Purified  
762 recombinant SARS-CoV-2 RBD was covalently immobilized on a sensor chip through its  
763 amine groups. Purified recombinant nanobodies flowed over the RBD individually at one  
764 of five different concentrations. The resulting data were fit to a 1:1 binding model and the  
765 value of  $K_d$  was calculated for each nanobody. The assay was repeated three times  
766 (biological replication: new aliquots of proteins and new sensor chips were used for each  
767 repeat).

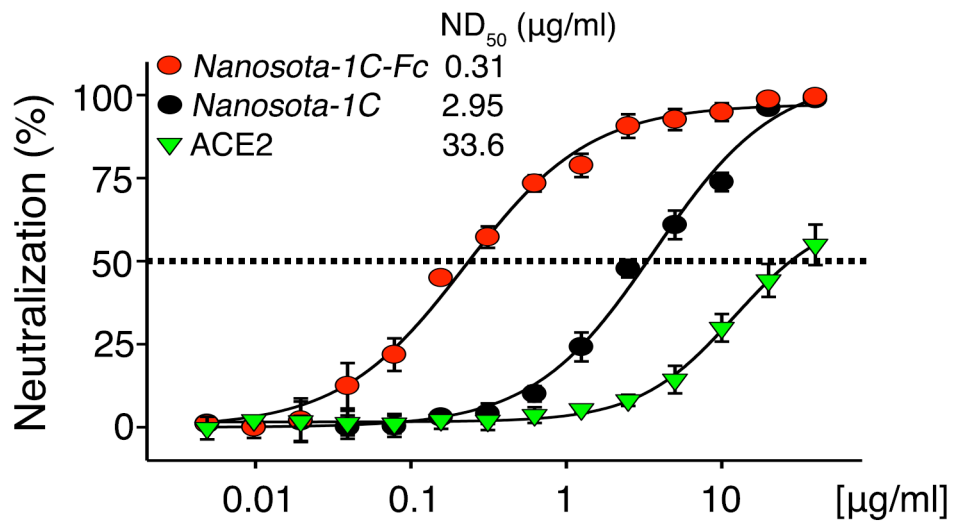
768



769

770 **Figure S4. Binding interactions between *Nanosota-1* drugs and SARS-CoV-2 RBD.**  
771 (A) Binding interactions between SARS-CoV-2 RBD, *Nanosota-1C*, and ACE2 as  
772 evaluated using a protein pull-down assay. Various concentrations of *Nanosota-1C* and a  
773 constant concentration of ACE2 (all His tagged) were combined in different molar ratios.  
774 SARS-CoV-2 RBD (Fc tagged) was used to pull down *Nanosota-1C* and ACE2. A  
775 western blot was used to detect the presence of *Nanosota-1C* and ACE2 following pull  
776 down by SARS-CoV-2 RBD. The assay was repeated three times (biological replication:  
777 new aliquots of proteins were used for each repeat). (B) Binding interactions between  
778 SARS-CoV-2 RBD, *Nanosota-1C*, and ACE2 as examined using gel filtration  
779 chromatography. *Nanosota-1C*, ACE2 and SARS-CoV-2 RBD (all His tagged) were  
780 mixed together in solution (both *Nanosota-1C* and ACE2 in molar excess of SARS-CoV-  
781 2 RBD) and purified using gel filtration chromatography. Protein components in each of  
782 the gel filtration chromatography peaks were analyzed with SDS-PAGE and stained by  
783 Coomassie blue. The assay was repeated three times (biological replication: new aliquots  
784 of proteins were used for each repeat).  
785

## SARS-CoV-2 (D614G) pseudovirus neutralization

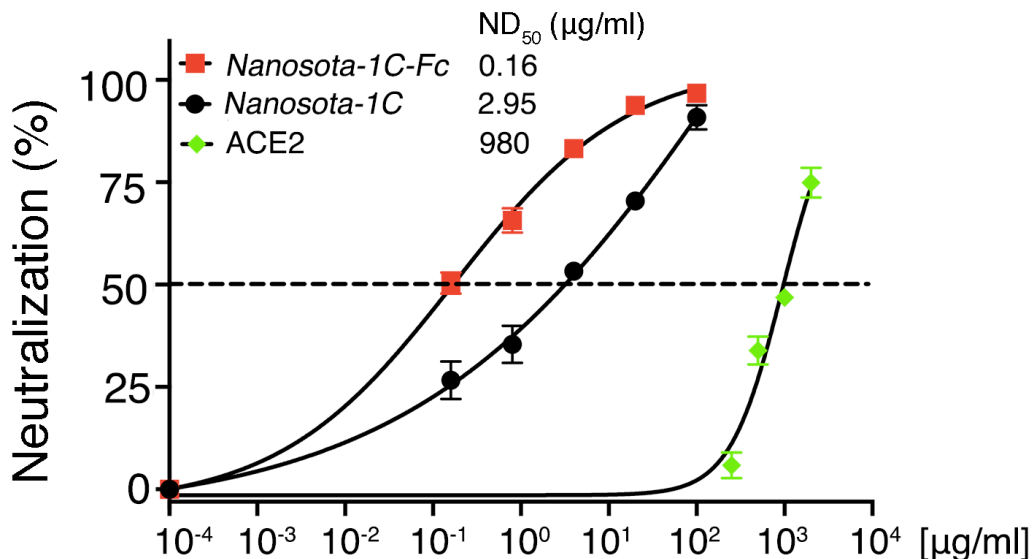


786

787 **Figure S5. Neutralization of SARS-CoV-2 pseudovirus, which contains the D614G**  
788 **mutation in the spike protein, by Nanosota-1 drugs.** The procedure was the same as  
789 described in Fig. 3A, except that the mutant spike protein replaced the wild type spike  
790 protein. The assay was repeated three times (biological replication: new aliquots of  
791 pseudoviruses and cells were used for each repeat).

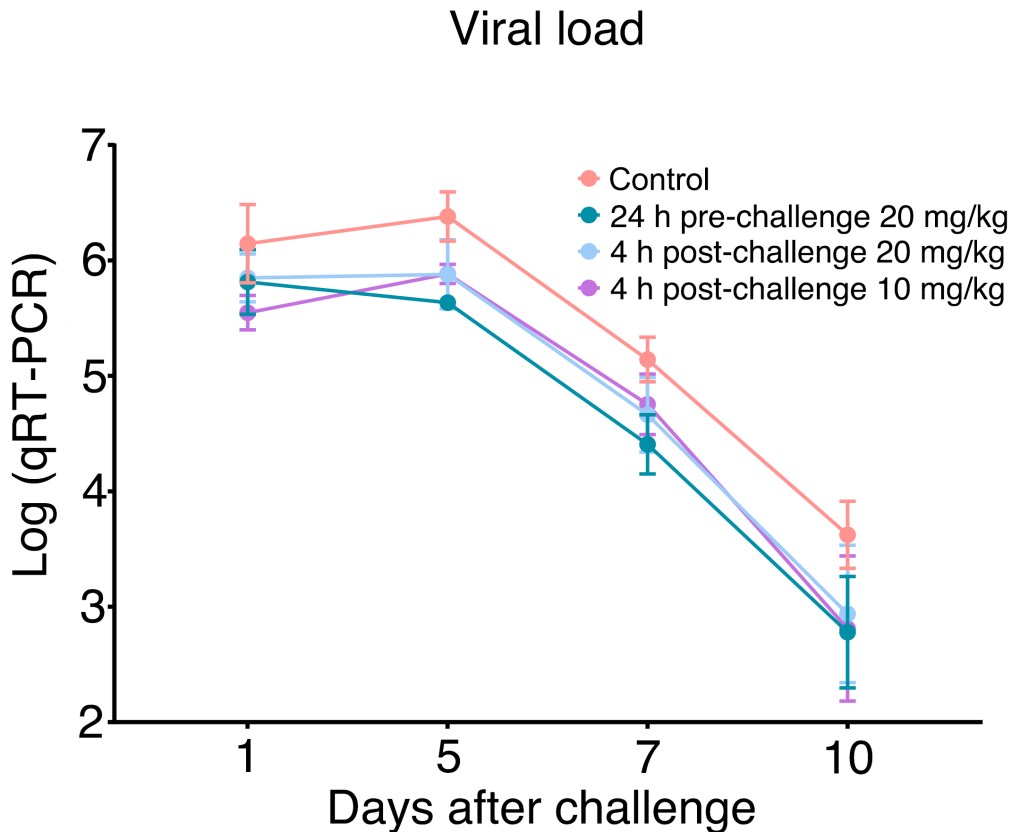
792

## Authentic SARS-CoV-2 neutralization

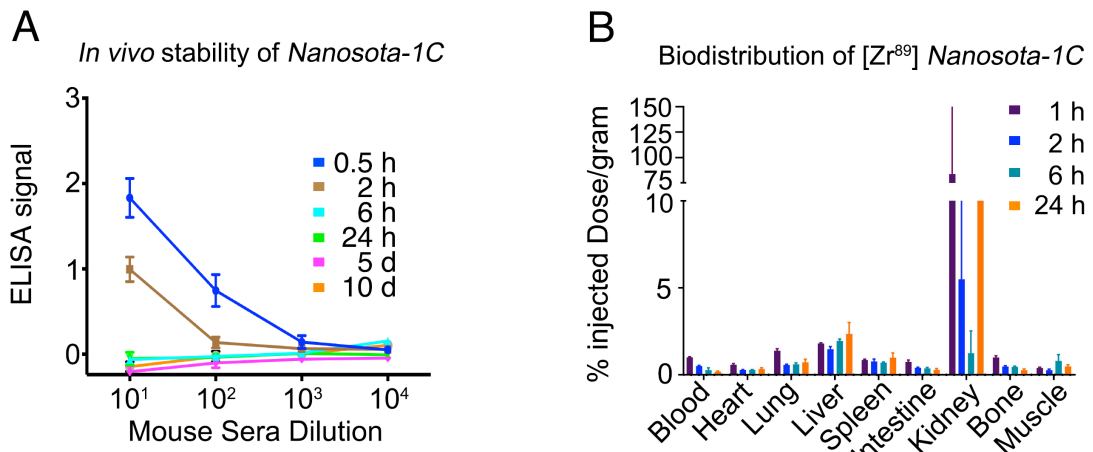


793

794 **Figure S6. Detailed data on the neutralization of authentic SARS-CoV-2 infection of**  
795 **target cells by Nanosota-1 drugs.** Data are the mean  $\pm$  SEM ( $n = 3$ ). Nonlinear  
796 regression was performed using a log (inhibitor) versus normalized response curve and a  
797 variable slope model ( $R^2 > 0.95$  for all curves). The assay was repeated twice (biological  
798 replication: new aliquots of virus particles and cells were used for each repeat).  
799



800  
801 **Figure S7. Additional data on the efficacy of Nanosota-1 drugs in protecting**  
802 **hamsters from SARS-CoV-2 infections.** Nasal swabs were collected from each hamster  
803 on days 1, 2, 3, 5, 7, and 10. Nasal swab samples from day 2 and day 3 were lost due to  
804 Hurricane Laura. qRT-PCR was performed to determine the virus loads in each of the  
805 samples. The qRT-PCR results are displayed on a log scale (since qRT-PCR amplifies  
806 signals on a log scale). Data are the mean  $\pm$  SEM ( $n = 6$ ). Missing data from one animal  
807 in the 4-hour post-challenge (10mg/kg) group on Day 7 were replaced by the average of  
808 that animal's days 5 and 10 data. ANOVA analysis using group as a between-group  
809 factor and day (1, 5, 7, and 10) as a within-group factor revealed significant differences  
810 between the control group and each of the following groups: 24 hour pre-challenge (20  
811 mg/kg) group ( $F(1, 10) = 6.02, p = .017$ , effect size  $\eta_p^2 = .38$ ), 4 hour post-challenge (20  
812 mg/kg) group ( $F(1, 10) = 5.38, p = .037, \eta_p^2 = .31$ ), and 4 hour post-challenge (10 mg/kg)  
813 group ( $F(1, 10) = 3.40, p = .048, \eta_p^2 = .25$ ). All  $p$ -values are one-tailed for directional  
814 tests.  
815



816  
817 **Figure S8. Pharmacokinetics of Nanosota-1C.** *In vivo* stability and biodistribution of  
818 Nanosota-1C were measured in the same way as described in Fig. 5C and Fig. 5D,  
819 respectively, except that time points for Nanosota-1C differed from those for Nanosota-  
820 IC-Fc due to pharmacokinetic differences of the small molecular weight nanobody  
821 versus the larger Fc tagged nanobody.  
822